

Maximum Energy of Particles in Plasmas

MITSUO OKA ¹, KAZUO MAKISHIMA ^{2,3} AND TOSHIO TERASAWA ⁴

¹Space Sciences Laboratory, University of California Berkeley, 7 Gauss Way, Berkeley, CA 94720, USA

²Department of Physics, The University of Tokyo, 7-3-1 Hongo, Bunkyo-ku, Tokyo 113-0033, Japan

³Kavli Institute for the Physics and Mathematics of the Universe (WPI), The University of Tokyo, 5-1-5 Kashiwa-no-ha, Kashiwa, Chiba 277-8683, Japan

⁴Institute for Cosmic Ray Research, The University of Tokyo, 5-1-5 Kashiwa-no-Ha, Kashiwa, Chiba 277-8582, Japan

ABSTRACT

Particles are accelerated to very high, non-thermal energies in space, solar, and astrophysical plasma environments. In cosmic ray physics, the *Hillas limit* is often used as a rough estimate (or the necessary condition) of the maximum energy of particles. This limit is based on the concepts of one-shot direct acceleration by a system-wide motional electric field, as well as stochastic and diffusive acceleration in strongly turbulent environments. However, it remains unclear how well this limit explains the actual observed maximum energies of particles. Here we show, based on a systematic review, that the observed maximum energy of particles — those in space, solar, astrophysical, and laboratory environments — often reach the energy predicted by the Hillas limit. We also found several exceptions, such as electrons in solar flares and jet-terminal lobes of radio galaxies, as well as protons in planetary radiation belts, where deviations from this limit occur. We discuss possible causes of such deviations, and we argue in particular that there is a good chance of detecting ultra-high-energy (~ 100 GeV) solar flare electrons that have not yet been detected. We anticipate that this study will facilitate further interdisciplinary discussions on the maximum energy of particles and the underlying mechanisms of particle acceleration in diverse plasma environments.

Keywords: Space plasmas (1544) — Plasma astrophysics (1261) — Solar flares (1496) — Cosmic rays (329) — Heliosphere (711) — Planetary magnetospheres (997)

1. INTRODUCTION

Particles — both ions and electrons — are accelerated to very high non-thermal energies in space, solar, and astrophysical plasma environments (e.g. Blandford & Eichler 1987; Terasawa 2001; Krucker et al. 2008; Oka et al. 2018, 2023; Guo et al. 2024, and references therein). While the mechanism of particle acceleration has been a topic of major debate, a significant question remains regarding the maximum particle energy that can be reached in each plasma environment.

In an effort to constrain potential origins of ultra-high-energy ($> 10^{18}$ eV) cosmic rays (UHECRs), Hillas (1984) argued that the size L_0 of the essential part of the acceleration region must be greater than $2r_g$, where r_g is the gyro-radius of UHECRs. If particles are accelerated stochastically, the diffusive motion needs a very large space, much larger than the gyro-radius, so that $L_0 > 2r_g/\beta$, where $\beta = V/c$ and V is the characteristic velocity of the scattering centers. Based on these considerations, Hillas (1984) presented what is now known as the Hillas diagram, which illustrates possible can-

didates of UHECR sources in the $B - L_0$ parameter space, where B is the magnetic field strength. It was proposed as a way to identify which sources fail to satisfy the requirements for UHECR sources.

Evidently, the arguments can be adapted in more generic discussions of maximum energy of particles in various plasma environments, well beyond the topic of search for UHECR production sites. The gyro-radius of relativistic particles is expressed as $r_g \sim \varepsilon/cqB$ (SI unit) where ε is the particle energy, c is the light speed, and q is the particle charge. Then, the condition of $L_0 > 2r_g$ gives the *hard* limit for the maximum particle energy achievable in a plasma environment:

$$\varepsilon_{\text{limit}} = qcBL \quad (1)$$

where we omitted the factor of 2 by introducing the half-width of the acceleration region $L = L_0/2$. A caveat here is that the statement $L > r_g$ is a necessary condition, rather than a sufficient condition, for particles to be trapped in the acceleration region. This is because particles might escape from the system even when $L > r_g$.

Hillas's second condition of $L_0 > 2r_g/\beta$ can be rewritten to provide a more stringent limit of the maximum energy of particles

$$\varepsilon_{\text{H}} = qVBL \quad (2)$$

which we hereafter refer to as the *Hillas limit*. While Hillas (1984) envisioned the stochastic acceleration scenario, the same expression can be obtained by assuming a one-shot, direct acceleration by the system-wide motional electric field VB . In fact, similar forms of Eq.(2) have been widely used in the context of magnetic reconnection where particles can be accelerated by the coherent reconnection electric field (e.g. Matthaeus et al. 1984; Goldstein et al. 1986; Martens 1988; Kliem 1994). Makishima (1999) also used such an idea of direct acceleration to arrive independently at the same scaling as Eq.(2), and argued that the predicted ε_H is often close to the highest particle energies ε_{obs} found in various plasma environments where not only magnetic reconnection but also shocks could play a major role.

Interestingly, Terasawa (2001) obtained essentially the same limit as Eq.(2) by assuming more explicitly that particles are accelerated stochastically in a diffusive environment. Using the spatial diffusion coefficient D , the size of the acceleration region can be roughly expressed as $\lambda = D/V$ (e.g. Blandford & Eichler 1987). If we normalize D by the Bohm diffusion coefficient $D_B = (1/3)r_g v$ (where v denotes the particle speed) and introduce $\eta \equiv D/D_B$, we obtain $\lambda = \eta D_B/V = \eta \varepsilon / 3qVB$ where we used the relativistic gyro-radius. Then, from the condition $\lambda \leq L$, we obtain the maximum attainable energy as

$$\varepsilon_{\text{diffusive}} = \frac{3}{\eta} qVBL \quad (3)$$

In the strong scattering limit ($\eta = 1$), this maximum energy is a factor of 3 higher than ε_H , although η is likely much larger than unity in solar and space plasmas. In the non-relativistic regime, we can readily obtain $\varepsilon_{\text{diffusive}} = (3/2\eta)qVBL$ which is still comparable to ε_H in the strong scattering limit. Therefore, we should keep in mind that Eq.(2) implies not only one-shot direct acceleration scenario but also the stochastic acceleration scenario.

A crucial point to note is that Eq.(2) remains a necessary, but not a sufficient, condition (e.g. Ptitsyna & Troitsky 2010; Kotera & Olinto 2011; Alves Batista et al. 2019; Matthews et al. 2020). More stringent conditions may arise from additional processes. In fact, Hillas (1984) already discussed, for example, possible compositions of UHECRs, associated transport processes, and energy losses due to synchrotron radiation. More up-to-date descriptions of the limitation factors for the maximum particle energy are well summarized by Matthews et al. (2020), particularly their Figure 5. In other words, with the understanding that the Hillas limit is a ballpark estimate, the cosmic ray physics community has sought more restrictive conditions in each plasma environment.

In contrast, Makishima (1999) and Terasawa (2001, 2011) took a different approach, aiming to validate the Hillas limit itself by comparing it with observations of high-energy particles and photons. They suggested that particle energies do reach the Hillas limit in various acceleration regions, even in solar and space plasma environments. On the other hand, a recent study suggests that the Hillas limit may overestimate observed maximum energies in many plasma environments

(Chien et al. 2023). Regardless, these studies did not fully account for additional loss processes considered in the context of UHECR studies.

This Paper presents a novel study that integrates both approaches. Leveraging more recent observations of space, solar, astrophysical, and laboratory plasmas, we first attempt to validate the Hillas limit itself. However, when interpreting the results, we consider radiative energy losses as well as the scattering intensity, parameterized by η . A large value of η represents weak scattering, less effective confinement of particles in the acceleration region, and therefore a condition more restrictive than the Hillas limit. We also treat ions and electrons separately. This is because, although the Hillas limit does not depend on the particle mass, ions and electrons could experience different acceleration and energy loss processes. Additionally, we try to use consistent definitions for V , B , and L for all plasma environments. With these new approaches, we have achieved a much better understanding of the maximum energy of particles in plasmas.

We first describe the methodology including the definitions of the V , B , L parameters (Section 2), followed by detailed descriptions of how we collected and compiled the parameter values, as well as the observed maximum energies of particles (Section 3). Then, we compare the observations and predictions in graphs (Section 4), discuss the results (Section 5), and conclude at the end (Section 6).

2. METHODOLOGY

We conducted a systematic review of the literature to deduce the key parameters (V , B , and L), predict the maximum particle energies ε_H via Eq.(2), and compare these predictions with the highest, observed energies of protons ($\varepsilon_{\text{obs,p}}$) and electrons ($\varepsilon_{\text{obs,e}}$). We selected plasma environments from which we can confidently derive these key parameters as well as ε_{obs} . While heavy ions are also observed in some cases, we focus on protons in this study for simplicity.

There are three caveats when conducting this study. The first is that, in many cases, the observed maximum energies (ε_{obs}) represent only a lower limit of the possible maximum particle energy. This is because the higher-energy cutoff in power-law spectra is often unclear, particularly in solar and space plasmas. Power-laws with exponential cut-offs (Ellison & Ramaty 1985; Band et al. 1993; Liu et al. 2020) can be found in, for example, Solar Energetic Particle (SEP) events (e.g. Ellison & Ramaty 1985; Mewaldt et al. 2012) and crossings of Earth's bow shock (e.g. Oka et al. 2006; Amano et al. 2020). However, observed energy spectra do not always exhibit such a cutoff feature in many plasma environments. The ε_{obs} values are typically derived from the highest energy channel of instruments that registered significant particle or photon counts. These values may be updated in the future with improved measurements that feature a larger energy range and higher sensitivity (or a larger dynamic range). Additionally, in the case of astrophysical objects, radiative energy losses could reduce the actual maximum energy of particles (Ptitsyna & Troitsky 2010). Therefore, ε_{obs} values

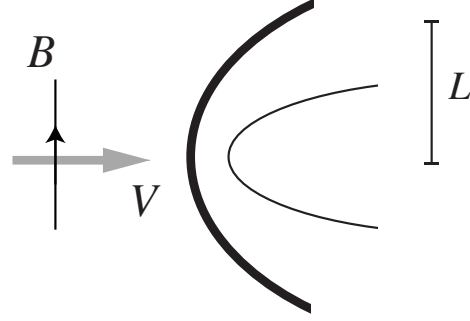
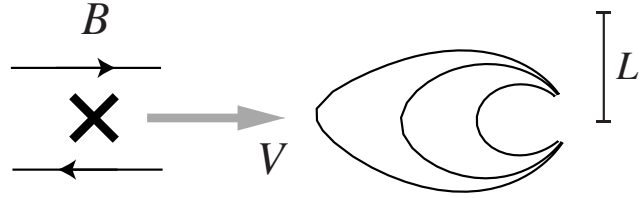
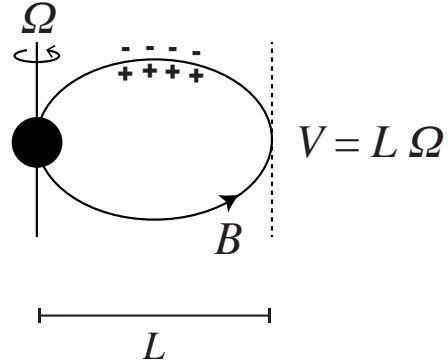
TYPE 1**Energy source:** Bulk flow V : upstream flow speed B : upstream magnetic field L : half-width (curvature radius) of the structure**Examples:** Planetary bow shocks, supernova remnant shocks, pulsar wind termination shocks, and hotspots in radiogalaxy lobes**TYPE 2****Energy source:** Magnetic field V : typical speed of fast flows B : upstream and asymptotic magnetic field L : half-width of the structure**Examples:** Planetary magnetotails and radiation belts, and solar/stellar flares**TYPE 3****Energy source:** Rotation of magnetized body V : maximum co-rotation speed B : magnetic field at the edge of co-rotation L : radius of the co-rotating plasma**Examples:** Jupiter's magnetosphere and pulsar magnetospheres

Figure 1. Schematic illustration of different types of plasma environments. Annotated on the left of each illustration are (1) the primary source of energy, (2) our definitions of V , B , and L , and (3) example plasma environments. This categorization is not meant to restrict the acceleration mechanism. For example, in the Type 2 environment, particles may be accelerated not only by magnetic reconnection but also by the termination shock formed by the dissipation of reconnection jets at the apex of a flaring loop. For more details, see Section 2 and Table 1.

that are lower than the Hillas limit do not automatically invalidate Eq.(2). Similarly, ε_{obs} values that are comparable to the Hillas limit ε_{H} do not necessarily confirm its validity, as the actual maximum energy could be exceeding the Hillas limit. However, $\varepsilon_{\text{obs}} \sim \varepsilon_{\text{H}}$ provides a strong evidence for particle acceleration mechanisms capable of reaching the Hillas limit energies.

Second, while direct *in-situ* measurements are available for space plasmas, remote-sensing measurements provides the key for diagnosing astrophysical plasmas. The observed maximum energy of photons can be identified, but it needs to be converted to the corresponding particle energy after knowing the emission mechanism and relevant parameters. For ex-

ample, synchrotron radiation depends on the magnetic field B , and so we need to treat the estimation of both B and ε_{obs} as a set of simultaneous equations.

Finally, V , B , and L should be defined in a way that is as consistent as possible across different plasma environments. As described in previous section, the Hillas limit can imply both one-shot direct acceleration and stochastic acceleration. Also, it does not necessarily distinguish shocks and magnetic reconnection. Therefore, we prefer to have a definition that does not explicitly depend on a specific acceleration mechanism. Nevertheless, the plasma condition and geometry differ greatly from acceleration site to site. To define V , B , and L , it is therefore still convenient to categorize plasma

environments based on the type of primary source of energy. Figure 1 illustrates the categorization and our definitions of V , B , and L .

The first type of plasma environment (Fig.1, top) has the upstream bulk flow as the primary source of energy. Examples include planetary bow shocks and the termination shocks of the heliospheric solar wind, pulsar winds, and jets in radio galaxies. This configuration does not necessarily mean particles are accelerated by shocks only. It is certainly possible that particles are accelerated by magnetic reconnection that occurs, for example, in the current sheets embedded in solar and pulsar winds (e.g. Drake et al. 2010; Zank et al. 2014, 2015; Lu et al. 2021). We define V as the bulk flow speed on the upstream side and B as the strength of the magnetic field carried by the flow. In astrophysical non-thermal sources, a magnetic field strength may be obtained through observations of emissions from the post-shock region, but we regard such a value as the magnetic field on the downstream side. Upon application of the Hillas limit, we reduce such a post-shock value by dividing by the shock compression ratio to derive the upstream value. The spatial scale L is approximated by the curvature radius of the shock front. In case of shell-type supernova remnants, we use the radius of the shell instead of the thickness of the shell, although we also provide thickness-based estimates for reference. In case of a radio galaxy, twin jets from its nucleus terminate via shocks, to form gigantic radio lobes filled with energetic particles. Although the shock front itself may not be spatially resolved via imaging in any wavelengths, we can still use the radius of the so-called hot-spots that sit at lobe centers which is clearly visible in radio images. In terrestrial/planetary bow shocks, the curvature radius could roughly correspond to the half-width of the obstruction, i.e., the magnetotail. It should also be roughly comparable to the standoff distance between the nose of the shock and the central planet.

The second type of plasma setting (Fig.1, center) has accumulated magnetic flux in the upstream region as the primary source of energy. In such a situation, the inflowing anti-parallel fields reconnect to produce bi-directional jets, one of which impinges on quasi-stationary magnetic fields anchored to some thick materials. Examples include solar flares and Earth’s magnetosphere. This categorization does not necessarily mean we exclude the possibility of other particle acceleration mechanisms. In solar flares, it is certainly possible that particles are accelerated by the termination shocks located at or above the top of the magnetic loop on the downstream side (e.g. Masuda et al. 1994; Tsuneta & Naito 1998; Chen et al. 2015). We define B as the characteristic (asymptotic) magnetic field on the upstream side of reconnection, such as the lobe magnetic field in Earth’s magnetotail and ambient magnetic field in the solar corona. We define V as the typical speed of the fast flows in the system to obtain an estimate of the maximum attainable energy in the system. It should be comparable to the reconnection outflow speed or the Alfvén speed V_A . Planetary radiation-belts also falls into this category. Although the solar wind dynamic pressure could be contributing to a global-scale compression of the

inner magnetosphere and hence particle energization in the radiation belts, observations also indicate that a substantial amount of particle and energy flux is ‘injected’ into the inner magnetosphere from the magnetotail.

The third type of plasma configuration involves a rapidly rotating, strongly magnetized planet or star, with the electric potential induced by the co-rotating magnetic field. Examples include the magnetospheres of Jupiter and pulsars such as the Crab Pulsar. While the precise mechanisms of particle acceleration remain unclear in such environments, a thin layer of charge separation which we refer to as a double-layer is often considered. As in the former two categories, the acceleration could also be driven by other mechanisms, such as magnetic reconnection and pitch angle scattering by waves. We define V as the maximum co-rotation speed, L as the radial distance from the central object to the location of the maximum co-rotation speed, and B is the typical magnetic field near the radial distance of L .

3. DATA COLLECTION

Based on the methodology described above, we searched the literature and collected data, as summarized in Table 1. In this section, we describe the details of the collected data.

3.1. Space Plasmas

Let us start from Earth’s magnetotail because it has been extensively investigated over the past decades. To estimate ε_H , we consider ‘near-Earth’ reconnection that takes place in the down-tail distances of $\sim 15 - 25R_E$ where R_E is Earth’s radius (e.g. Miyashita et al. 2009). In this region, the lobe magnetic field is $B = 15 - 25$ nT (Fairfield & Jones 1996) and the half-width of the magnetotail is $L = 15 - 25R_E$ or $(9.6 - 16) \times 10^7$ m (Fairfield 1971). For the speed V , we use the typical speed of bursty bulk flows $V = 300 - 1000$ km s⁻¹ in the central plasma sheet (e.g. Angelopoulos et al. 1992; Zhang et al. 2016). While the flow channel appears to be much narrower than the full width of the magnetotail, on the order of a few R_E (e.g. Angelopoulos et al. 1996), we adhere to our definition described in Section 2 and use the magnetotail half-width for L . Consequently, we obtain $\varepsilon_H = 0.4 - 4.0$ MeV, while earlier observations have reported up to ~ 1 MeV for both ions and electrons (e.g. Terasawa & Nishida 1976; Krimigis 1979; Christon et al. 1988, 1989, 1991). A recent study also reported a detection of ~ 2 MeV electrons that were precipitating into Earth’s atmosphere from the magnetotail (Artemyev et al. 2024). It is worth noting that earlier studies already argued that the direct acceleration by the reconnection electric field does not explain \sim MeV particles (e.g. Terasawa & Nishida 1976; Krimigis 1979). In fact, the polar cap potential, which is formed when the dayside magnetopause reconnection enables the solar wind to drive ionospheric convection, is known to saturate only at ~ 200 kV (Hairston et al. 2005; Shepherd 2007).

Earth’s radiation belt is also a distinct region of particle acceleration, but the values of B vary largely and the val-

Table 1. The Hillas limit and the observed maximum energy of particles in various plasma environments.

Plasma environment		Flow speed	Magnetic field	System Size	Hillas limit	Observations	
Type	Name	V (km s ⁻¹)	B (nT)	L (m)	ϵ_H	$\epsilon_{\text{obs,p}}$	$\epsilon_{\text{obs,e}}$
2	Earth’s magnetotail	300 – 1000	15 – 25	$(9.6 - 16) \times 10^7$	0.4 - 4 MeV	1 MeV	2 MeV
2	Earth’s radiation belt	300 – 1000	15 – 25	$(9.6 - 16) \times 10^7$	0.4 - 4 MeV	800 MeV	15 MeV
1	Earth’s bow shock	400 – 600	5 – 8	$(9.6 - 16) \times 10^7$	190 - 760 keV	300 keV	300 keV
2	Mercury’s magnetosphere	300 – 400	40 – 50	$(4.9 - 9.8) \times 10^6$	59 - 200 keV	550 keV	300 keV
3	Jupiter’s radiation belt	400 – 800	5 – 15	$(5.2 - 8.2) \times 10^9$	10 - 98 MeV	80 MeV	100 MeV
3	Saturn’s radiation belt	200 – 500	5 – 10	$(1.2 - 2.9) \times 10^9$	1 - 15 MeV	300 MeV	2 MeV
1	Saturn’s bow shock	300 – 600	0.2 – 1.0	$(2.9 - 3.5) \times 10^9$	0.2 - 2 MeV	–	700 keV
1	Heliosphere (ACR)	250 – 350	0.02 – 0.1	$(1.2 - 1.8) \times 10^{13}$	60 - 630 MeV	100 MeV	–
2	Solar flares	1000 – 3000	$(5 - 50) \times 10^6$	$(1.0 - 3.0) \times 10^7$	0.05 - 5 TeV	30 GeV	45 MeV
1	CME (shock)	1000 – 4000	300 – 10000	$(3.5 - 10) \times 10^9$	1 - 420 GeV	30 GeV	–
1	SN 1006	2700 – 4600	0.1 – 0.5	2.7×10^{17}	73 - 620 TeV	100 TeV	10 TeV
1	RX J1713.7-3946	3900	0.1 – 1.0	1.4×10^{17}	53 - 530 TeV	100 TeV	100 TeV
1	Crab Nebula	3×10^5	1 – 4	4.3×10^{15}	2 - 6 PeV	–	2 PeV
3	Crab Pulsar	3×10^5	1.0×10^{11}	1.5×10^6	45 PeV	–	15 TeV
1	Cygnus A	72000 – 90000	9 – 10	$(3.4 - 4.6) \times 10^{19}$	22 - 42 EeV	–	30 GeV
1	Laser plasma (shock p)	1500	2.0×10^{10}	$(3.0 - 4.0) \times 10^{-3}$	90 - 120 keV	80 keV	–
1	Laser plasma (shock e-)	1000	1.0×10^{11}	5.0×10^{-3}	500 keV	–	500 keV
2	Laser plasma (mrx e-)	500 – 1100	5.0×10^{10}	1.0×10^{-3}	25 - 55 keV	–	40 – 70 keV

NOTE— The first column shows the type of each environment (either 1, 2, or 3). See Section 2 for more details. The plasma environments are listed in the order of appearance in Section 3. The average radii of the planets are as follows: Earth $R_E \sim 6.371 \times 10^6$ m, Mercury $R_M \sim 2.440 \times 10^6$ m, Jupiter $R_J \sim 6.9911 \times 10^7$ m, and Saturn $R_S \sim 5.8232 \times 10^7$ m. The average solar radius is $\sim 6.957 \times 10^8$ m. For unit conversions, 1 nT = 10 μ G.

ues of V can be fluctuating around ~ 0 due to its oscillatory motion, making it difficult to choose a characteristic value of B and V . Therefore, we use the characteristic values in the magnetotail, as also described in Section 2. This is because, while electrons can be accelerated locally inside the radiation belt, a substantial fraction of their energy originates from the magnetotail in the forms of waves and moderately accelerated seed particles (e.g. Jaynes et al. 2015; Sorathia et al. 2018; Turner et al. 2021, and references therein). The highest energies of observed particles are ~ 800 MeV for protons (Mazur et al. 2023) and ~ 15 MeV (or possibly higher) for electrons (Blake et al. 1992; Vampola & Korth 1992). However, such high-energy protons are likely to be supplied by galactic cosmic rays (GCRs). It has been known that GCR particles knock neutrons out from the atmospheric atoms and such neutrons decay to produce protons (e.g. Singer 1958a,b; Hess 1959; Li et al. 2023). This is called Cosmic Ray Albedo Neutron Decay (CRAND). More details of CRAND are discussed in Section 5.4.

For Earth’s bow shock, we consider the typical values of the ‘fast’ solar wind at 1 AU (e.g. Larrodera & Cid 2020), i.e., $B = 5 - 8$ nT and $V = 400 - 600$ km s⁻¹. The system

size L should be roughly the same as that of the magnetotail, $L = 15 - 25 R_E$, or $(9.6 - 16) \times 10^7$ m. As a result, we expect $\epsilon_H \sim 190 - 760$ keV, while observations in the shock upstream region find energetic protons of up to ~ 300 keV (e.g. Scholer et al. 1981; Turner et al. 2018; Trattner et al. 2023) and electrons of similar energies (e.g. Wilson et al. 2016), although these energetic protons may be partially contributed by those from the magnetosphere (Scholer et al. 1981). A recent observation of hot flow anomalies — transient concentrations of shock-reflected, supra-thermal ions that occur when a certain structures in the solar wind collide with the bow shock — reported energizations of ions (Turner et al. 2018). In their report, the energy spectrum of H⁺, He²⁺, and O⁶⁺ extended up to ~ 100 , ~ 300 , and ~ 600 keV, while showing a peak at ~ 30 , ~ 120 , and ~ 300 keV, respectively. While the authors successfully interpreted the peak energies by a Fermi-type acceleration ‘trap’ between two converging magnetic mirrors, such a dependence on charge state could also be attributed to Eq.(2).

In Mercury’s magnetosphere with its half-width being $L \sim 2 - 4 R_M$ where R_M is Mercury’s radius or $(4.9 - 9.8) \times 10^6$ m (Winslow et al. 2013), protons of up to ~ 550 keV (Simp-

son et al. 1974) and electrons of up to ~ 300 keV (Simpson et al. 1974; Ho et al. 2011, 2012; Lawrence et al. 2015) have been detected. The magnetotail reconnection appears to occur around $\sim 3R_M$ down-tail, and the lobe magnetic field in such a region is $\sim 40 - 50$ nT (Poh et al. 2017; Bowers et al. 2024). The bulk flow speed V has been neither directly nor routinely measured, but we assume $300 - 400$ km s $^{-1}$ based on flow speeds associated with dipolarization (Dewey et al. 2018) and flux ropes (FTEs) (Slavin et al. 2012). This is comparable to the estimated thermal speed of ions (Raines et al. 2011). As a result, we obtain $\varepsilon_H = 59 - 200$ keV.

Jupiter’s plasma environment is very different from those of rocky planets such as Earth and Mercury. Its dynamics is largely driven by the rapid planetary rotation, assisted by the significant internal mass loading from the volcanic moon Io (e.g. Jackman et al. 2014; Guo & Yao 2024, and references therein). A key picture here is that, at a certain distance from the central planet, the magnetic field is stretched outward and the co-rotation breaks down due to magnetic reconnection (Vasyliunas 1983). This is consistent with Type 3 illustrated in Figure 1, and we use the typical radial distance at which the magnetic reconnection takes place, i.e., $L \sim 90 - 140R_J$ where R_J is Jupiter’s radius, or $(5.2 - 8.2) \times 10^9$ m (Vogt et al. 2010, 2020). The lobe magnetic field at such radial distances is $5 - 15$ nT (Kivelson & Khurana 2002) and the typical speed of fast plasma flows is $V \sim 400 - 800$ km s $^{-1}$ (Kronberg et al. 2008). As a result, we obtain $\varepsilon_H = 10 - 98$ MeV. For observation, synchrotron emissions from $\gtrsim 50$ MeV electrons in the radiation belt was first reported by Bolton et al. (2002), and it was suggested that there is a maximum cutoff at ~ 100 MeV (de Pater & Dunn 2003). We also add that non-thermal bremsstrahlung X-rays of up to 20 keV have been detected from the polar (auroral) regions of Jupiter (Mori et al. 2022). For protons, the maximum observed energy of ~ 80 MeV was recorded near the main ring of Jupiter (Fischer et al. 1996; Kollmann et al. 2017). Notably, heavy ions of $\gtrsim 125$ MeV are also detected based on ionization signatures in the star camera onboard the Juno spacecraft (Becker et al. 2021).

Saturn’s plasma environment is in many ways intermediate between those of Earth and Jupiter (Jackman et al. 2014). However, the effect of planetary rotation appears to be dominant (e.g. Guo & Yao 2024) and so we consider Saturn’s magnetosphere as one of the third type described in Section 2. On average, the X-line is located at distances of $20 - 30R_S$ where R_S is Saturn’s radius, but it is highly variable and could be located as far out as $\sim 50R_S$ (McAndrews et al. 2009; Smith et al. 2016). Thus, we adopt the spatial scale of $L = 20 - 50R_S$, or $(1.2 - 2.9) \times 10^9$ m. The lobe magnetic field in such locations is $5 - 10$ nT (Jackman et al. 2014). With the possible flow speeds $V = 200 - 500$ km s $^{-1}$ (e.g. Hill et al. 2008; McAndrews et al. 2009), we obtain $\varepsilon_H = 1 - 15$ MeV. In reality, protons with energies up to at least ~ 300 MeV (e.g. Roussos et al. 2018; Krupp et al. 2018) and electrons up to at least ~ 2 MeV (e.g. Paranicas et al. 2010; Roussos et al. 2014) have been observed in Saturn’s radiation belt. Here, the high-energy protons are likely CRAND protons that also exist in Earth’s radiation belt.

At Saturn’s bow shock, electrons up to ~ 700 keV were detected when the solar wind Alfvén Mach number M_A was unusually high ~ 100 (Masters et al. 2013). Based on the solar wind parameters at Saturn, i.e., $B = 0.2 - 1.0$ nT and $V = 300 - 600$ km s $^{-1}$ (e.g. Masters et al. 2013; Thomsen et al. 2019; Gershman et al. 2024), as well as the half-width of the magnetosphere $L = 50 - 60R_S$, or $(2.9 - 3.5) \times 10^9$ m (e.g. McAndrews et al. 2009; Jackman et al. 2019), we estimate $\varepsilon_p = 0.2 - 2$ MeV.

For the heliosphere, we consider Anomalous Cosmic Rays (ACRs) that appear as an excess flux in the lowest energy range of the galactic cosmic ray spectra (e.g. Giacalone et al. 2022, and references therein). In today’s standard scenario, neutral particles of interstellar origin are ionized deep inside the heliosphere and then ‘picked-up’ by the solar wind to be transported back toward the outer edge of the heliosphere. They are likely accelerated by the heliospheric termination shock to become ACRs, although the precise acceleration mechanism has been a topic of debate, especially after recent observations by Voyagers 1 and 2. The energies of ACR protons can reach ~ 100 MeV (e.g. Cummings & Stone 1998). Jokipii & Giacalone (1998) already argued that these highest energies are gained from electrostatic potential while drifting along the shock surface, which they estimated as $200 - 300$ MeV. In our case, we use $B = 0.02 - 0.1$ nT and $V = 250 - 350$ km s $^{-1}$ as they were measured just upstream of the termination shock by the Voyager spacecraft (Burlaga et al. 2008). For L , we use the expected average distance between the Sun and the termination shock along the ‘nose’ direction, i.e., $80 - 120$ AU, or $(1.2 - 1.8) \times 10^{13}$ m. As a result, we obtain $\varepsilon_H = 60 - 630$ MeV.

3.2. Solar Plasmas

In solar flares, the Bremsstrahlung emission from energetic electrons produces the X-ray/ γ -ray continuum up to a few tens of MeV (e.g. Lin et al. 2002). In such remote-sensing measurements, the precise evaluation of the maximum energy of electrons is confounded by the photons produced by the decay of pions (e.g. Vilmer et al. 2003). However, *in-situ* measurements reported ~ 45 MeV electrons from solar flares (Evenson et al. 1984; Moses et al. 1989).

To estimate ε_H for solar flares, we consider spatially-large flares that fit into the standard model where magnetic reconnection in the corona plays a major role (e.g. Masuda et al. 1994; Shibata et al. 1995). This is a Type 2 plasma environment. We therefore adopt the values of V and B in the corona, even though a large part of flare emission originates from the chromospheric footpoints of flaring loop. For the flow speed V , we assume the typical Alfvén speed, $1000 - 3000$ km s $^{-1}$ (e.g. Aschwanden 2005). For the magnetic field, we assume $(5.0 - 50) \times 10^6$ nT, or $B = 50 - 500$ G (e.g. Aschwanden 2005; Chen et al. 2020). For the system size L , we assume $L = 10 - 30$ Mm, or $(1.0 - 3.0) \times 10^7$ m, which is half the loop-size of spatially-large flares (e.g. Aschwanden et al. 1996; Aschwanden 2005; Krucker et al. 2008; Oka et al. 2015). Alternatively, we could use the length of flare arcade (or flare ribbon) that extends in the direction of reconnection

electric field. It can be ~ 200 Mm or even larger. However, we keep the definition outlined in Section 2 and use the flare loop size. In fact, hard X-ray sources are usually isolated or fragmented and do not extend along the flare arcade (e.g. Asai et al. 2002; Shi et al. 2024), suggesting that the acceleration region do not extend as long as the length of the arcade. With these parameters, we obtain $\varepsilon_H = 0.05 - 5$ TeV.

For high-energy protons of solar origin, we consider observations by ground-based, cosmic-ray monitors. During solar eruptive events including solar flares and coronal mass ejections (CMEs), significant enhancements of GeV proton flux are observed, which are referred to as Ground Level Enhancements (GLEs) (e.g. Carmichael 1962). To date, protons of up to ~ 30 GV in rigidity (approximately 30 GeV in energy) have been detected (Lovell et al. 1998). One intriguing aspect of these observations is that the spectra often exhibit a roll-off, indicating that the power-law spectra are unlikely to extend further, even with improved measurements of GLEs. Therefore, we do not consider the observed value of 30 GeV as a lower limit.

Unfortunately, the origin of GLE protons remains ambiguous. They can be produced by solar flares (in which magnetic reconnection plays an important role), CME-associated shocks, or both (Kahler 1994; Vashenyuk et al. 2011; Aschwanden 2012; Guo et al. 2023; McCracken et al. 2023). Some observations and modeling indicate that GLEs often exhibit a two-step evolution: a prompt enhancement possibly due to a solar flare, followed by a gradual decay possibly due to a CME shock (e.g. Vashenyuk et al. 2011). However, because of the lack of consensus on the origin, we assume that both solar flares and CMEs produce protons of ~ 30 GeV. It should be noted that recent observations by Fermi’s Large Area Telescope (LAT) reported γ -ray spectra that are consistent with the decay of pions produced by > 300 MeV protons (Ajello et al. 2021). They found at least two distinct types of γ -ray emission: prompt-impulsive and delayed-gradual, which could be related to the two-step evolution of GLE events.

To estimate ε_H for CMEs (and associated shocks), we take into account the statistical study by Kahler (1994). They reported that GLEs exhibited a peak when the height of associated CME reached $5 - 15R_\odot$ (Kahler 1994). Then, we use $L = 5 - 15R_\odot$, or $(3.5 - 10) \times 10^9$ m, combined with $B = 300 - 10000$ nT, or $0.003 - 0.1$ G (Bird & Edenhofer 1990), and $V = 1000 - 4000$ km s $^{-1}$ (Smart & Shea 1985), to obtain $\varepsilon_H = 1 - 420$ GeV for CMEs in Table 1.

3.3. Astrophysical Plasmas

3.3.1. SN 1006

Supernova remnants (SNRs) are one of the most important astrophysical plasma environments in the context of the Hillas limit. This is because SNRs are promising sites for cosmic ray production up to the ‘knee’ energy (\sim TeV) or even beyond, and whether they can actually achieve this energy has been a subject of intense debate, both observationally and theoretically (e.g. Lagage & Cesarsky 1983; Bell

2004; Hillas 2005; Drury 2012; Suzuki et al. 2022; Diesing 2023; Tao et al. 2024).

The Hillas limit ε_H for SN 1006 is obtained as follows, using our definitions for Type 1 environment. The remnant of SN 1006 exhibits a shell structure with the average radius of $\sim 15'$ (e.g. Gardner & Milne 1965; Koyama et al. 1995; Bamba et al. 2003). Using the distance of ~ 2 kpc (e.g. Green 2019; Winkler et al. 2003) where $1 \text{ pc} = 3.1 \times 10^{16}$ m, we have $L \sim 2.7 \times 10^{17}$ m. The remnant is interpreted as a shock front expanding at the speed of $0''.28 - 0''.48$ per year (Winkler et al. 2003; Katsuda et al. 2009) or $2700 - 4600$ km s $^{-1}$. For the upstream magnetic field, we use the typical interstellar magnetic field of $0.1 - 0.5$ nT, or $1 - 5\mu\text{G}$. As a result, we obtain $\varepsilon_H \sim 73 - 620$ TeV.

It should be noted that a higher value of ε_H can be obtained by focusing on the local conditions at the shock front. In the diffusive shock acceleration scenario (e.g. Blandford & Eichler 1987), particles are accelerated within a finite region around the shock front. Consequently, the thickness of the shell measured in X-rays and γ -rays, approximately $1'$ (Bamba et al. 2003; Li et al. 2018), should correspond to the spatial extent of the acceleration region (e.g. Yamazaki et al. 2004). For the magnetic field B , recent observations have found evidence for a highly amplified value at the shell, $B \gtrsim 20$ nT (Tao et al. 2024), consistent with earlier expectations (e.g. Berezhko et al. 2002; Parizot et al. 2006). Therefore, by adopting $B \sim 20$ nT and $L \sim 1'$, or 1.8×10^{16} m, we obtain a predicted maximum energy $\varepsilon_H \sim 2$ PeV. This is an order of magnitude higher than our first estimate.

Let us turn to the observational estimates ε_{obs} , using X-ray and gamma-ray remote sensing. The observed X-ray spectra exhibit a clear cutoff at a photon energy of ~ 0.2 keV, which can be interpreted as synchrotron emission from electrons with the maximum energy of 10 TeV in a magnetic field of 1 nT (Bamba et al. 2008). On the other hand, observed γ -rays can be attributed to the inverse Compton scattering by electrons off photons of cosmic microwave background (CMB), or proton-induced pion-decay, or a combination of both. Based on a hybrid model that takes into account both mechanisms of γ -ray production, it has been reported that the maximum energies of electrons and protons are $\varepsilon_{\text{obs,e}} \sim 10$ TeV and $\varepsilon_{\text{obs,p}} \sim 100$ TeV, respectively, with a magnetic field strength of 4.5 nT (Acero et al. 2010). These energies match with our estimates within an order of magnitude.

3.3.2. RX J1713.7-3946

RX J1713.7-3946 is another shell-forming SNR, roughly $30'$ in diameter at the distance of ~ 1 kpc (e.g. Tsuji & Uchiyama 2016), giving us $L \sim 1.4 \times 10^{17}$ m. The expansion speed is 3900 km s $^{-1}$ (Tsuji & Uchiyama 2016), which we use for V . A key difference from SN 1006 is that it is located right on the Galactic plane where the interstellar medium is much denser and possibly non-uniform. In fact, a part of the shell is moving substantially slower, indicating an ongoing interaction with local clouds (Tanaka et al. 2020). Furthermore, the presence of dense interstellar material appears to enable the so-called hadronic channel, in which ac-

celerated protons collide with ambient protons to produce pions. These pions subsequently decay into a pair of 70 MeV (in rest frame) gamma-ray photons, thereby contributing significantly to the observed flux of gamma-ray emission. For the upstream magnetic field, we assume 0.1 - 1 nT, which includes values slightly higher than those we used for SN 1006, considering the presence of denser materials. Then, we predict the maximum energy of particles as $\varepsilon_H \sim 53 - 530$ TeV, very similar to that of SN 1006. Alternatively, we can again consider the local condition with amplified magnetic field of $B \sim 10$ nT (Uchiyama et al. 2007) and shell thickness $L \sim 0.5'$ (Tanaka et al. 2020) to obtain $\varepsilon_H \sim 170$ TeV, a value consistent with the above estimation.

For observations, the spectra have been measured with both X-rays (e.g. Takahashi et al. 2008; Yuan et al. 2011; Tsuji et al. 2019) and γ -rays (e.g. Abdo et al. 2011; Yuan et al. 2011; Abdalla et al. 2018). The observed maximum energy of particles is obtained as $\varepsilon_{\text{obs,p}} \sim \varepsilon_{\text{obs,e}} \sim 100$ TeV, although it can vary within an order of magnitude depending on the spectral model employed, including how much fraction of ions contribute to the photon emissions (*hadronic* versus *leptonic*). In this regard, a recent study that takes into account the column density of the local interstellar medium concludes that ions and electrons constitute about 70% and 30% of the total γ -ray emissions, respectively (Fukui et al. 2021). This result provides valuable evidence for proton acceleration in astrophysical settings.

3.3.3. Crab Nebula

The Crab Nebula is also a supernova remnant, but the presence of a spinning pulsar at its center makes it very different from more ordinary shell-type SNRs (e.g. Longair 2011; Buhler & Blandford 2014, and references therein). A distinctive feature in its X-ray image is the torus and the associated inner ring (Weisskopf et al. 2000), which is interpreted as the termination shock formed as the pulsar wind — a magnetized, relativistic flow of electrons and positrons from the pulsar — collides with the surrounding nebula (Kennel & Coroniti 1984). To estimate ε_H , we use the radius of the inner ring ~ 0.14 pc, or 4.3×10^{15} m (Weisskopf et al. 2000) for L and the light speed $c \sim 3 \times 10^5$ km s $^{-1}$ for V . The magnetic field B in the post-shock region can be estimated from the spectral break that appears in the synchrotron spectrum at $\nu \sim 10^{13}$ Hz. Assuming that the spectral break represents the condition of the synchrotron cooling time being comparable to the age of the nebula, we can obtain $B \sim 30$ nT (Marsden et al. 1984). Similar estimates in the range of 10 – 30 nT have been obtained by other studies (e.g. Buhler & Blandford 2014, and references therein). To further estimate the magnetic field in the upstream region of the shock, we adopt the compression ratio 7 for a relativistic, strictly perpendicular shock and obtain $B \sim 1 - 4$ nT. Combining the parameters, we obtain the Hillas limit of $\varepsilon_H \sim 2 - 6$ PeV.

Regarding observations, the electromagnetic spectrum from Crab Nebula has been observed over a wide range of energies from radio to γ -ray ranges, revealing both components of synchrotron and inverse Compton emissions (e.g. Zhang

et al. 2020; Aharonian et al. 2024). According to these observations, the synchrotron component exhibits a clear cutoff at the photon energy of ~ 50 MeV. Using the magnetic field 30 nT obtained above and the formula for the synchrotron critical frequency, we find that this photon energy corresponds to an electron energy of $\varepsilon_{\text{obs,e}} \sim 2$ PeV. The inverse Compton component extends beyond 0.1 PeV (Aharonian et al. 2024), which corresponds to the electron energy of $\varepsilon_{\text{obs,e}} \sim 0.5$ PeV. However, the cutoff is not visible in the spectra and so we regard this value as a lower-limit of $\varepsilon_{\text{obs,e}}$.

It should be noted that there may be a non-negligible contribution to the spectrum from energetic protons, although the leptonic model has been widely accepted (e.g. Atoyan & Aharonian 1996). In this regard, a recent broad-band spectral analysis considered hadronic photons from the neutral pion-decay process and showed that the fraction of energy converted into energetic protons is likely $< 0.5\%$ although it could be as high as 7% if only the γ -ray data are used (Zhang et al. 2020). Therefore, we consider that the plasma in the Crab Nebula consists of predominantly electrons and positron. Consequently, we did not include protons in Table 1.

3.3.4. Crab Pulsar

The Crab Pulsar is not spatially resolved by remote-sensing measurements, and much of our evaluation of the Hillas limit is based on the arguments and parameters described in classical literature (e.g. Goldreich & Julian 1969; Longair 2011; Buhler & Blandford 2014). The Crab Pulsar produces intense beams of radiation through acceleration of particles within its magnetosphere. The particle acceleration mechanism remains largely unknown, and there exist different models, such as polar cap, outer gap, and slot gap models, depending on the assumed location of the acceleration site. An important spatial scale in pulsar's magnetosphere is the radius of the light cylinder R_{LC} . This is where the speed of the magnetic field co-rotating with the pulsar reaches the light speed, so that $R_{LC} = c/\Omega \sim 1.5 \times 10^6$ m where $\Omega = 200$ rad s $^{-1}$ is the pulsar's angular velocity. Therefore, to estimate the predicted maximum energy of particles, we adopt the definitions for Type 3 environment and use $L = R_{LC}$ and $V = c \sim 3 \times 10^5$ km s $^{-1}$. For the magnetic field strength B , it scales like $\propto r^{-3}$ where r is the distance from the pulsar and $B \sim 4 \times 10^{17}$ nT, or 4×10^{12} G, at the equatorial surface of the neutron star. Thus, we obtain 10^{11} nT at the surface of the cylinder. Then, the predicted maximum energy becomes ~ 45 PeV.

The Crab Pulsar produces pulsed emissions, and photon spectra that extends up to \sim TeV have been measured, despite the flux being two orders of magnitude smaller than that of the nebula (Ansoldi et al. 2016; Yeung 2020). Assuming inverse Compton scattering off photons of cosmic microwave background (CMB), this maximum photon energy corresponds to the maximum particle energy of $\varepsilon_{\text{obs}} \sim 15$ TeV. We consider this as a lower-limit of ε_{obs} .

3.3.5. Cygnus A

As touched on in Section 2, jet-terminal lobes of radio galaxies (particularly of the so-called Fanaroff-Riley Type II, or FR-II) are also an interesting astrophysical environment. It is generally considered that particle acceleration occurs predominantly at the termination (reverse) shock, creating hot-spots in a central region of their radio lobes (e.g. Carilli & Barthel 1996; Casse & Marcowith 2005). In this study, we specifically consider Cygnus A (3C405) because it is one of the brightest radio galaxies and has been studied intensively from various approaches. Based on observations by, for example, Meisenheimer et al. (1997) and Steenbrugge & Blundell (2008), combined with our guideline for the Hillas limit (Section 2), we use the estimated radius of the hot-spots, $L = 1.1 - 1.5$ kpc, or $(3.4 - 4.6) \times 10^{19}$ m, and the jet speed of $V = (0.24 - 0.30)c$, or $72000 - 90000$ km s⁻¹. For the magnetic field B , we assume its value in the hot-spot 40 nT (Meisenheimer et al. 1997), and divide it by the shock compression ratio $3.9 - 4.3$ to obtain the shock upstream value $9 - 10$ nT. These numbers bring the predicted maximum energy ε_H very high, 22 - 42 EeV, up to the range of ultra-high-energy cosmic rays (UHECRs), \gtrsim EeV. In fact, radio galaxy lobes was one of the candidates for the site of UHECR production based on earlier evaluations of the Hillas limit (e.g. Hillas 1984; Rachen & Biermann 1993; Norman et al. 1995).

In contrast to the above predictions, the observed maximum energy of electrons is much lower, $\varepsilon_{\text{obs}} \sim 30$ GeV in the hot-spots of Cygnus A (Meisenheimer et al. 1997). Similar values of ε_{obs} have been obtained for the lobe regions (Steenbrugge & Blundell 2008; Yaji et al. 2010). This issue is not specific to Cygnus A, because FR-II radio galaxies generally show synchrotron emissions predominantly in the radio range and do not extend to the higher-energy X-ray range. The observations in the X-ray range are interpreted by the inverse Compton scattering off CMB photons by the relativistic electrons (e.g. Feigelson et al. 1995; Kaneda et al. 1995). Therefore, the observed maximum energies are robust, and it is clear that electrons do not reach the Hillas limit in the hot-spots of FR-II radio galaxies. We discuss this gap in Section 5.

3.4. Laboratory Plasmas

Laboratory experiments provide unique opportunities to study plasma phenomena in a controlled manner. In particular, recent developments in laser facilities have enabled experimental studies of particle acceleration at shocks and reconnection in a collisionless condition.

Yao et al. (2021) observed 80 keV protons at a shock front generated by a laser-driven, fast flow of plasma expanding into an ambient cloud of plasma. Using an earlier phase of the evolution when the shock front was still moving at a high speed, they evaluated the Hillas limit with the shock speed $V \sim 1500$ km, the shock size $L \sim (3 - 4) \times 10^{-3}$ m, and the ambient magnetic field 2×10^{10} nT, to obtain $\varepsilon_H \sim 90 - 120$ keV which is comparable to the observed energy.

Fiuza et al. (2020) detected 500 keV electrons at a shock front generated by an interaction of laser-driven, counter-streaming flows of plasma. They reported the Alfvén Mach

number $M_A \sim 400$. They also evaluated the Hillas limit with the following parameters: the flow speed $V \sim 1000$ km s⁻¹, the transverse size of the shock $L \sim 5 \times 10^{-3}$ m, and the magnetic field $\sim 10^{11}$ nT, or 1 MG, leading to the expected maximum energy of $\varepsilon_H \sim 500$ keV, well consistent with the observation.

Chien et al. (2023) reported a detection of 40–70 keV electrons during magnetic reconnection in a laser-driven plasma experiment. The reconnection geometry was formed by currents induced in two U-shaped coils by the same laser-driven plasma. During the initial ‘push’ phase, when the currents were still increasing, the reconnection was more strongly driven than compared to a later phase. Their simulations of this experiment indicated that the peak rate of reconnection was $\alpha_R \sim 0.6$ where α_R is defined as the inflow speed V_{in} normalized by the Alfvén speed V_A , i.e., $\alpha_R = V_{in}/V_A$. Using data from this earlier phase, along with the inferred peak value of $\alpha_R \sim 0.6$, they calculated the reconnection electric field to be $0.6V_A B_0$, where $V_A \sim 500 - 1100$ km s⁻¹ and $B_0 \sim 5 \times 10^{10}$ nT. With a system size of $\sim 10^{-3}$ m (or 1.4 times the ion inertia length), they derived a predicted maximum energy of 13-30 keV, which is roughly half the observed energy.

A caveat here is that this prediction was based on the inflow speed of $0.6V_A$, whereas our Hillas limit evaluation is based on the outflow speed, or equivalently V_A (Section 2). Thus, we estimate ε_H without the factor 0.6 and obtain $\varepsilon_H \sim 25 - 55$ keV, which is comparable to the observed values. It should also be noted that, according to Chien et al. (2023), the system size was so small that the observed reconnection was deeply in the electron-only regime, where ions are decoupled from the process and do not exhibit ion-scale jets (Phan et al. 2018). In the presented systematic review, this is the smallest physical system used for testing the Hillas limit.

4. RESULTS

All the values compiled in Table 1 are visualized in Figures 2 and 3 for protons and electrons, respectively. In both panels, the horizontal axis shows the maximum energy ε_H predicted by Eq.(2), derived from the parameters V , B , and L , whereas the vertical axis shows the observed maximum energy ε_{obs} . For those plasma environment in which ε_{obs} is the lower-limit of the observations, we added an upward arrow. The black solid line is the identify line of $\varepsilon_{\text{obs}} = \varepsilon_H$. It is labeled ‘direct’ because the Hillas limit can be interpreted by ‘direct’ (one-shot) acceleration.

The gray shaded area indicates ‘diffusive’ acceleration, as approximated by Eq.(3) and more accurately expressed as follows. The spatial diffusion coefficient is $D = V\lambda = \eta p v / 3qB$, where p is the particle momentum. The particle kinetic energy is $\varepsilon_{\text{obs}} = \sqrt{p^2 c^2 + m^2 c^4} - mc^2$. Then, from the condition of $\lambda \leq L$ where λ is the spatial scale of the acceleration region, combined with $\varepsilon_H = qVBL$, we eventually obtain the maximum energy from the case of $\lambda = L$ as

$$\varepsilon_{\text{obs}} = \varepsilon'_H + \sqrt{\varepsilon'^2_H + m^2 c^4} - mc^2 \quad (4)$$

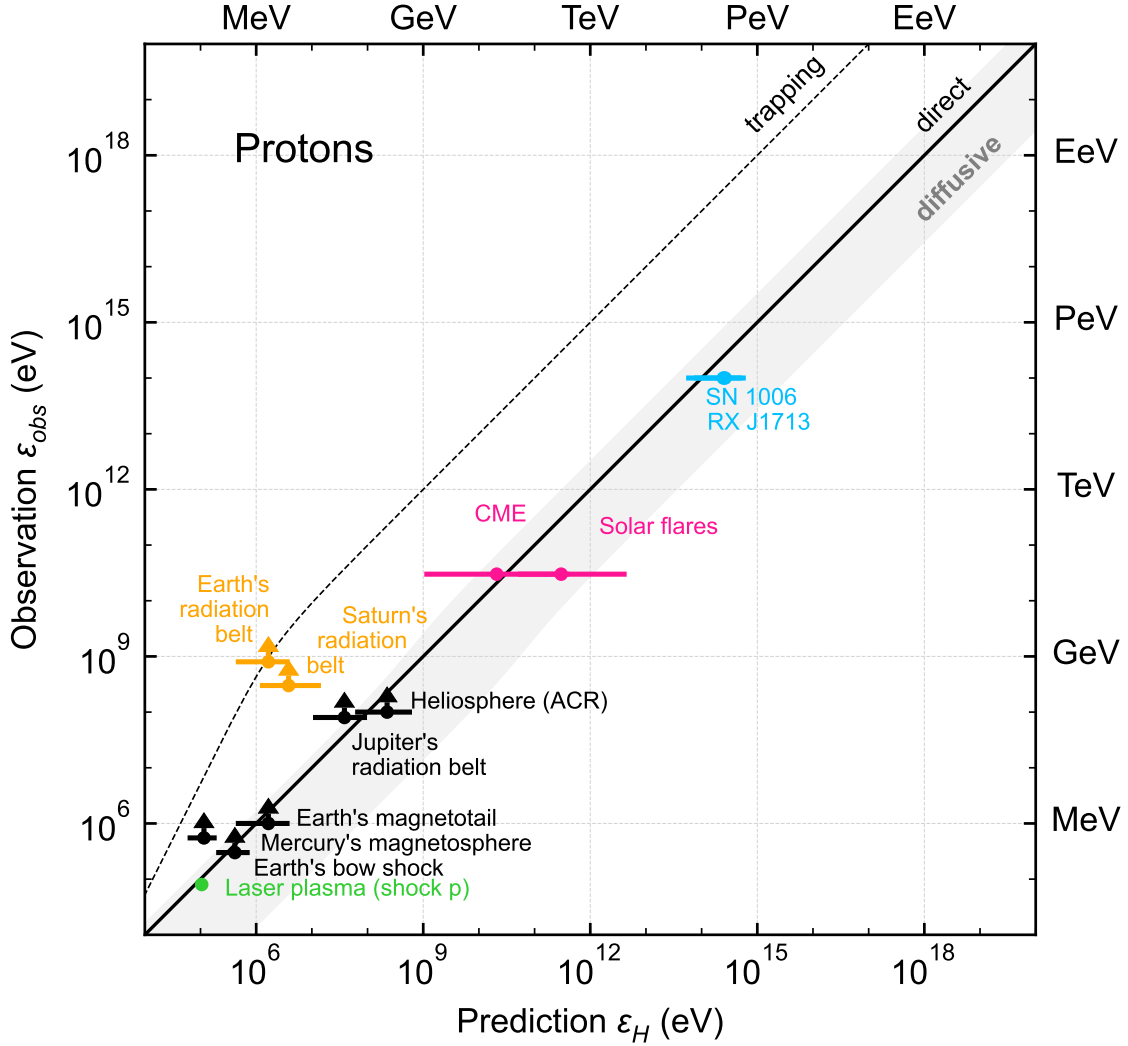


Figure 2. The maximum energy of protons in various plasma environments, as compared between the Hillas limit prediction (horizontal axis) and observations (vertical axis). See Table 1 for the values used and Section 3 for their justification. The black line is the identity line and represents the scenario of direct, one-shot acceleration. The gray shaded region represents the scenario of stochastic and diffusive acceleration with a strong scattering, $\eta = 1 - 100$. The dashed curve represents the trapping condition $r_g \leq L$ for the case of $\psi = c/V = 1000$ or $V = 300 \text{ km s}^{-1}$.

where $\varepsilon'_H = (3/2\eta)\varepsilon_H$. The shaded region in Figures 2 and 3 shows this condition with the range of $\eta = 1 - 100$. In the limit of $\varepsilon_H \gg mc^2$, this condition reduces to Eq.(3) or $\varepsilon_{\text{obs}} = (3/\eta)\varepsilon_H$.

The dashed line indicates the ‘trapping’ condition or the *hard* limit, as approximated by Eq.(1) and more accurately expressed as follows. From the condition of $r_g \leq L$ where $r_g = p/qB$ is the gyro-radius, we eventually obtain

$$\varepsilon_{\text{obs}} = \sqrt{\psi^2 \varepsilon_H^2 + m^2 c^4} - mc^2 \quad (5)$$

where $\psi = c/V$. The dashed curve in Figures 2 and 3 shows this condition with $\psi = 1000$. This corresponds to $V=300 \text{ km s}^{-1}$, which is close to the lower limit of the typical range of V in many plasma environment (See Table 1). In the limit

of $\varepsilon_H \gg mc^2$, Eq.(5) reduces to Eq.(1) or $\varepsilon_{\text{obs}} = \psi\varepsilon_H = \varepsilon_{\text{limit}}$.

It is evident from Figure 2 that the Hillas prediction generally agrees with the observed maximum energies of protons within an order of magnitude. An exception is the radiation belts at Earth and Saturn (orange), as their maximum energies substantially exceeds the Hillas limit (solid line). We consider this excess is due to externally-supplied CRAND protons. Their observed energies are still lower than or comparable to the hard limit (dashed line).

The Hillas prediction also agrees with the observed maximum energies of electrons within an order of magnitude, as shown in Figure 3, although there is a few large deviations. In Cygnus A, the observed maximum energy $\varepsilon_{\text{obs,e}}$ is nearly 9 orders of magnitude lower than the prediction. As described

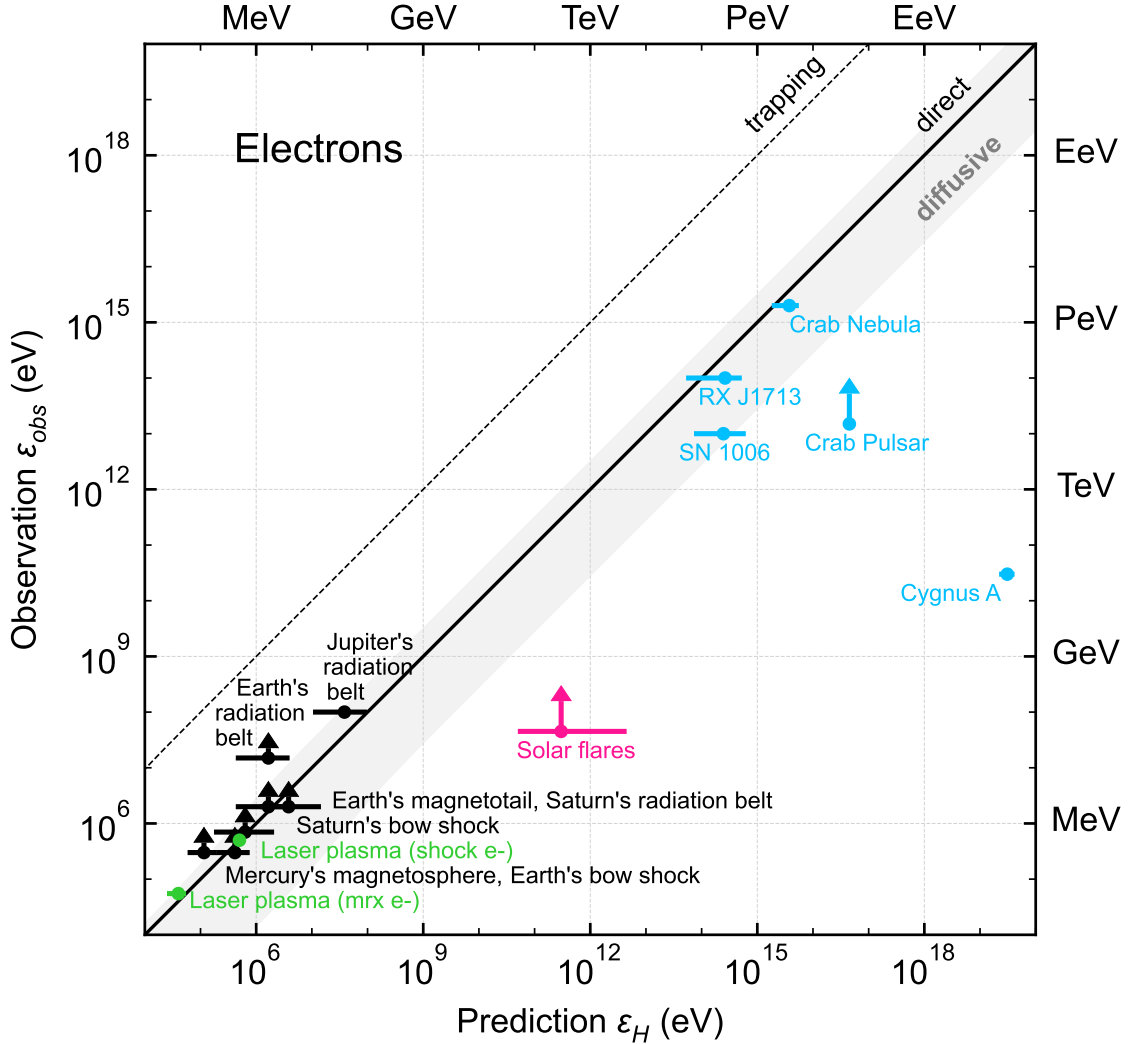


Figure 3. The maximum energy of electrons in various plasma environments, with the same format as Figure 2.

in Section 3.3, we do not consider this a lower limit. For solar flares and the Crab Pulsar, the deviation is roughly ~ 4 orders of magnitude, but the observed values can be regarded as a lower limit. Therefore, it is still possible that the particle energies do reach the Hillas limit in these environments.

To further evaluate the validity of the Hillas limit, we performed a multivariate analysis where the dependencies of the observed maximum energy ε_{obs} on the parameters V , B , and L are modeled as

$$\varepsilon_{\text{obs}} = DV^a B^b L^c \quad (6)$$

where D is a constant and the indices a , b , and c are free parameters to represent those dependencies. This is, in a sense, a purely empirical, bottom-up analysis with no prior knowledge of particle acceleration theories. Although some values of ε_{obs} are considered as lower limits, we took the logarithm of the above expression and performed a linear regression, treating all values equally, after removing obvious outliers: Earth's radiation belt and Saturn's radiation belt for protons

and solar flares, the Crab Pulsar, and Cygnus A for electrons. The resultant best-fit model for protons is

$$\varepsilon_{\text{obs,p}} = (9.6 \times 10^{-4}) V^{1.47 \pm 0.56} B^{0.79 \pm 0.10} L^{0.86 \pm 0.07} \quad (7)$$

It is evident that all indices are close to unity, indicating that the observed maximum energies of particle depend almost linearly on V , B , and L , consistent with Eq. (2). For electrons, we performed the same analysis and obtained

$$\varepsilon_{\text{obs,e}} = (2.6 \times 10^{-2}) V^{1.27 \pm 0.23} B^{0.78 \pm 0.09} L^{0.82 \pm 0.06} \quad (8)$$

Again, the indices are close to unity.

Therefore, we conclude that the Hillas Limit actually holds in many particle acceleration environments, even when the parameters B and L vary greatly across many orders of magnitude. However, we emphasize again that we treated all values equally, including those considered lower limits. Thus, these multivariate analysis results should be validated in the future as improved measurements of the maximum energy

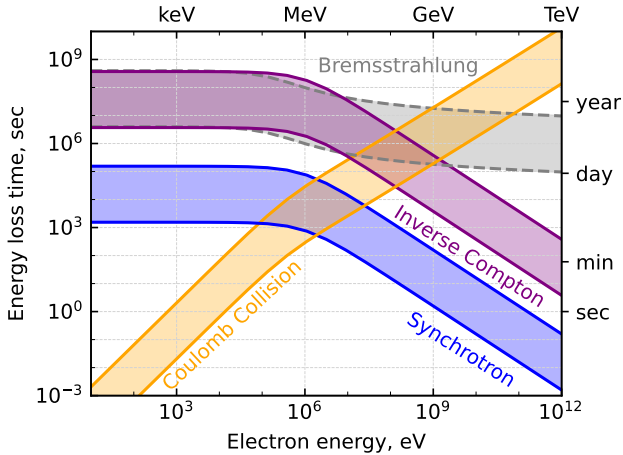


Figure 4. Energy loss time for fast electrons in the solar corona, demonstrating the importance of synchrotron cooling in the relativistic regime. Four different processes (as annotated) are considered with densities $n = 10^8 - 10^{10} \text{ cm}^{-3}$ and magnetic fields $B = (5 - 50) \times 10^6 \text{ nT}$, or $50 - 500 \text{ G}$. In the case of inverse Compton, we considered scattering off photons of solar origin instead of the Cosmic Microwave Background (CMB).

of particles become available. Additionally, we excluded known outliers that cannot be explained by the Hillas limit alone. For such outliers, additional physical processes must be considered, such as an external supply for protons and energy loss and weak scattering conditions for electrons. These topics are discussed in the next section.

5. DISCUSSION

While it has been established that accelerated non-thermal particles often exhibit a power-law spectrum, how far the power-law spectrum extends and what limits the particle energy have remained unclear. Here, in this study, we have confirmed earlier suggestions (Makishima 1999; Terasawa 2001) that the highest observed energy of particles ε_{obs} does reach the Hillas limit ε_{H} . In fact, they often match quite well, i.e., $\varepsilon_{\text{obs}} \sim \varepsilon_{\text{H}}$, over a very wide range of parameters, despite the fact that many of the observed values should be regarded as lower limits. The multivariate analysis that treat all ε_{obs} values equally returned indices that are consistent with the Hillas limit expressed as Eq.(2). This universal scaling law becomes even more impressive when we recall the earlier argument that the Hillas limit, which initially appears as a one-shot direction acceleration by a system-wide electric field (Eq.(2)), can actually be interpreted within the scenario of stochastic and diffusive acceleration with strong scattering (Terasawa 2001), as expressed in Eq.(3). Furthermore, the *hard* limit based on the condition of $r_g \leq L$ also appears to nicely explain a few cases of planetary radiation belt that clearly exceeded the Hillas limit. In this section, we first explore the possible implications of this scaling law on the underlying mechanism of particle acceleration. We then discuss some of the deviations from the Hillas limit that we have

identified in our systematic review of the maximum energy of particles.

5.1. Particle Acceleration Mechanisms

We emphasize that it is possible for a stochastic acceleration to work simultaneously with energization by the system-wide motional electric field. This is perhaps most clearly described by Jokipii (1987) who showed theoretically that, if the cross-field diffusion is sufficiently strong across a quasi-perpendicular shock, particles can be energized as they drift along the $\mathbf{V} \times \mathbf{B}$ electric field while experiencing diffusive shock acceleration, resulting in a higher rate of energy gain than in the case of a quasi-parallel shock.

It has also been suggested that both coherent and stochastic components of acceleration work for particle acceleration in MHD turbulence due to magnetic reconnection (e.g. Ambrosiano et al. 1988; Dmitruk et al. 2003). In their work, a normalized version of Eq.(2) is used, following Matthaeus et al. (1984), and the system size L is replaced with the Alfvén transit time τ_A . Then, it was demonstrated with test particle simulations that, as τ_A increases, the maximum energy of particles also increases in MHD turbulence (Dmitruk et al. 2003).

Similarly, two-dimensional (2D), full particle simulations have shown that the highest energy of particles is matched with the prediction of $qE_R\Delta Z$ where q is the particle charge, E_R is the reconnection electric field, and ΔZ is the displacement of particles in the direction of the reconnection electric field (See Figure 11 of Oka et al. (2010)). The match was observed in simulations of multi-island coalescence where particles change their direction of motion (and thus experience scattering) at the merging point. More formal treatment of particle acceleration in quasi-2D interacting magnetic islands can be found in, for example, Zank et al. (2014). A key point here is that the same effect might take place in 3D magnetic reconnection with turbulence. Therefore, we speculate that, even in a turbulent and diffusive environment, a small number of fortuitous particles can still experience energization while moving across the system as implied by the Hillas limit.

5.2. Electrons in Radio Galaxy Lobes

While it is difficult to distinguish the two different acceleration mechanisms with our dataset alone, more detailed investigations of radio galaxy lobes (including the hot spots) might provide an important clue. This is because there is a strikingly large discrepancy between ε_{obs} and ε_{H} for electrons in Cygnus A. The gap is roughly 9 orders of magnitude. Such a large gap exists in other FR-II radio galaxies as well, and it has been an important subject of research (e.g. Casse & Marcowith 2005; Araudo et al. 2018, and references therein). It was argued that the observed maximum energy cannot be explained by synchrotron cooling even after considering magnetic field amplification at the shock front and that the hot-spots of FR-II radio galaxies are indeed poor accelerators of particles (Araudo et al. 2016, 2018).

This is in stark contrast to the Heliosphere (ACR) and the Crab Nebula where particles are accelerated at a reverse shock, similar to hot-spots of radio galaxies, and yet the maximum energies of particles reach very close to the Hillas limit. At and around the termination shock of the Heliosphere and the Crab nebula, magnetic reconnection could occur frequently due to the intrinsic presence of current sheets in the solar and pulsar winds. Such current sheets, when compressed by the termination shock, can lead to enhanced turbulence via magnetic reconnection and associated particle acceleration (e.g. Drake et al. 2010; Zank et al. 2014, 2015; Lu et al. 2021). On the other hand, jets in radio galaxies do not necessarily carry current sheets, although the precise magnetic field structure within the jets is unknown. We therefore conjecture that magnetic reconnection is lacking at the termination shock of radio-galaxy hot-spots, thereby reducing the chance of particle scattering by reconnection-induced turbulence.

Further investigations of magnetic field structure in the hot-spots may lead to a better understanding of the gap between observations and the Hillas limit of the maximum energy of particles of radio lobes, and more generally, to a deeper insight into the particle acceleration mechanisms in various plasma environments.

5.3. Electrons in Solar Flares

The maximum energy of electrons in solar flares is also much smaller than what is predicted by the Hillas limit. This is particularly important because protons do reach the energy much closer to the Hillas limit prediction. It should be emphasized again that the highest energy electrons of solar origin were observed by *in-situ* measurements that are limited by the sensitivity and energy coverage of the instrument. In general, measuring high energy electrons in space is more difficult than measuring protons, due to various reasons including the effect of background noise (secondary electrons) caused by high-energy protons. Therefore, it is important to continue improving the diagnostics of high-energy electrons of solar origin. If we determine there really is a large discrepancy between the Hillas limit and the observed maximum energy of electrons, it indicates that a physical process that is unique to electrons, either acceleration or energy loss, is at play. Because electrons reach the Hillas limit energy levels in many space plasma environments and there is no reason to believe turbulence is weaker in solar plasmas than in space plasmas, we tentatively consider the possibility that the maximum energy of solar electrons is limited by radiative energy losses.

Figure 4 shows the timescale of different energy-loss processes, as a function of electron energy, obtained by using formulas summarized by Longair (2011). For Coulomb collisions, we used a formula provided by Saint-Hilaire & Benz (2005). It is evident that, while collisions dominate in the non-relativistic regime, energy loss by synchrotron emission dominates in the relativistic regime (See also Appendix of Krucker et al. 2008).

In fact, the timescale of synchrotron energy loss for a particle of energy ε is expressed as

$$\tau_{\text{synch}} \sim 38 \left(\frac{B}{100 \text{ G}} \right)^{-2} \left(\frac{\varepsilon}{\text{GeV}} \right)^{-1} \text{ sec} \quad (9)$$

This is shorter than the typical duration of large-scale impulsive flares (\sim minutes) but longer than that of X-ray pulsations (~ 0.5 s) which are thought to be individual sequences of energy-release (e.g. Aschwanden 2005).

This can also be compared to the energy loss time due to inverse Compton scattering off photons of solar origin. With the solar luminosity of $L_{\odot} = 3.83 \times 10^{33} \text{ erg s}^{-1}$, its energy density at the solar surface is $L_{\odot}/4\pi R_{\odot}^2 c = 1.31 \times 10^{18} \text{ eV m}^{-3}$. Then, the energy loss time is

$$\tau_{\text{IC},\odot} \sim 7 \times 10^3 \left(\frac{\varepsilon}{\text{GeV}} \right)^{-1} \text{ sec} \quad (10)$$

Similarly, if we consider inverse Compton scattering off CMB photons with an energy density of $2.65 \times 10^5 \text{ eV m}^{-3}$, the energy loss time is

$$\tau_{\text{IC,CMB}} \sim 4 \times 10^{16} \left(\frac{\varepsilon}{\text{GeV}} \right)^{-1} \text{ sec} \quad (11)$$

These timescales are much larger than that of energy loss by synchrotron emission (see also Figure 4), and electron energies could reach the Hillas limit if they were to lose energy only by the inverse Compton emission. Therefore, synchrotron emission remains as the possible mechanism of radiative energy loss during electron acceleration in the solar corona.

Now, if we consider the one-shot direct acceleration by the electric field $E \sim VB$ in the corona, where $V \sim 3000 \text{ km/s}$ and $B \sim 100 \text{ G}$, we can readily see that electrons would reach relativistic energies and travel over the distance of $L \sim 20 \text{ Mm}$ almost instantly within $\sim 9 \times 10^{-5} \text{ s}$. Therefore, the energy loss by synchrotron is negligible in the direct acceleration scheme.

This is not necessarily the case for the diffusive acceleration scheme from which Eq.(3) is derived. The acceleration timescale is $\sim D/V^2$, and the condition $D/V^2 \lesssim \tau_{\text{synch}}$ gives us

$$\varepsilon_{\text{diffusive}} \lesssim \frac{100}{\sqrt{\eta}} \left(\frac{B}{100 \text{ G}} \right)^{-\frac{1}{2}} \left(\frac{V}{3000 \text{ km/s}} \right) \text{ GeV} \quad (12)$$

This indicates that the electron energy will still have no problem reaching the Hillas limit, 0.05 – 5 TeV, depending on the parameters B and V , in the strong scattering limit of $\eta \sim 1$. However, in a pessimistic case of $B \sim 500 \text{ G}$, $V \sim 1000 \text{ km s}^{-1}$, and $\eta \sim 10^4$, the electron energy might be limited to $\sim 150 \text{ MeV}$, only a few times higher than the highest energy currently observed, 45 MeV.

In summary, for solar flare electrons, the discrepancy between the observed maximum energy and the Hillas limit can be explained by the synchrotron energy loss, but the synchrotron limit depends on the parameters V , B , and L . In

particular, the parameter values of V and B can vary depending on the observation methodology and the height of plasma from the solar surface. Based on Eq.(12), there is still a good chance of detecting ultra-high-energy (up to $\gtrsim 100$ GeV) solar flare electrons that have not yet been detected. We call for further efforts to achieve better *in-situ* measurements of high-energy, solar flare electrons with higher sensitivity and wider energy coverage. We hope that future measurements can more clearly identify the higher-energy cutoff in the energy spectra, just like the roll-off energies seen in proton spectra during GLEs.

5.4. Protons in Planetary Radiation Belts

In contrast to the above cases of discrepancy where electron energies fall well below the Hillas limit, proton energies that substantially exceed the Hillas limit have been observed in the radiation belts of Earth and Saturn (Figure 2). As mentioned earlier, these protons can be explained by CRAND (e.g. Singer 1958a,b; Hess 1959; Li et al. 2023). The GCR-induced neutrons produce protons, electrons, and antineutrinos through β decay, but protons carry the largest energy and are trapped in the radiation belts. Interestingly, proton energies do not exceed the Hillas limit as much in Jupiter’s radiation belt. In fact, it has already been argued that CRAND is weak in Jupiter’s radiation belt (Kollmann et al. 2017). In Jupiter’s plasma environment, particles are continuously supplied from the volcanic moon Io (e.g. Jackman et al. 2014; Guo & Yao 2024, and references therein). Heavier ions rather than protons are the main constituent, while CRAND only provides protons and electrons. Therefore, it is not surprising that we have not seen enhanced flux of highest energy protons beyond the Hillas limit.

6. CONCLUSION

We tested the Hillas limit using recent results of observations of various plasma environments, combined with renewed, consistent definitions of the key parameters V , B , and L . We found that particles do reach the Hillas limit in many cases, confirming earlier findings (Makishima 1999; Terasawa 2001). However, there were some exceptions. Ac-

celerated electrons in the FR-II radio galaxy Cygnus A are 9 orders of magnitude less energetic compared to the Hillas limit predictions. We speculate that this is due to possible absence of magnetic reconnection in the hot-spots and that scattering is too weak to achieve acceleration up to the Hillas limit. Similarly, in solar flares, electrons have been observed with energies up to tens of MeV, which is well below the energy predicted by the Hillas limit. We suggest that electrons with much higher energies could be detected with improved instrumentation, although there is a possibility that the energy is limited by synchrotron cooling. On the other hand, the maximum energy of protons in planetary radiation belts clearly exceeds the Hillas limit due to externally supplied CRAND protons.

It should be noted that Chien et al. (2023) already argued that there is a large gap between observations and the Hillas limit in many different plasma environments, where magnetic reconnection may play a major role (Type 2). In this study, we focused only on plasma environments from which we could confidently derive key parameters V , B , and L , as well as the observed maximum energy ε_{obs} . Consequently, our list contained many plasma environments where shocks are likely playing a major role in energy conversion (Type 1 in Figure 1 and Table 1). A more comprehensive test of the Hillas limit with a larger number of Type 2 plasma environments is left for future studies, and we anticipate more interdisciplinary discussions of the maximum energy of particles that use both theoretical and observational approaches.

We benefited from discussions with many experts from various fields. We particularly thank Hantao Ji for valuable discussions in the early stage of this study, Lyndsay Fletcher for drawing our attention to synchrotron cooling in solar plasma, and Shunsaku Nagasawa for his help in estimating the timescales of radiative losses. We also thank Drew L. Turner for providing relevant references on radiation belts, Christopher C. Chaston and Soléne Lejosne for their helpful discussions on the same topic, and Katsuaki Asano for his valuable input on the Crab Nebula flares. MO was supported by NASA grants 80NSSC18K1002 and 80NSSC22K0520 at UC Berkeley.

REFERENCES

- Abdalla, H., Abramowski, A., Aharonian, F., et al. 2018, *Astronomy & Astrophysics*, 612, doi: [10.1051/0004-6361/201629790](https://doi.org/10.1051/0004-6361/201629790)
- Abdo, A. A., Ackermann, M., Ajello, M., et al. 2011, *The Astrophysical Journal*, 734, doi: [10.1088/0004-637x/734/1/28](https://doi.org/10.1088/0004-637x/734/1/28)
- Acero, F., Aharonian, F., Akhperjanian, A. G., et al. 2010, *Astronomy & Astrophysics*, 516, doi: [10.1051/0004-6361/200913916](https://doi.org/10.1051/0004-6361/200913916)
- Aharonian, F., Ait Benkhali, F., Aschersleben, J., et al. 2024, *Astronomy & Astrophysics*, 686, doi: [10.1051/0004-6361/202348651](https://doi.org/10.1051/0004-6361/202348651)
- Ajello, M., Baldini, L., Bastieri, D., et al. 2021, *The Astrophysical Journal Supplement Series*, 252, 13, doi: [10.3847/1538-4365/abd32e](https://doi.org/10.3847/1538-4365/abd32e)
- Alves Batista, R., Biteau, J., Bustamante, M., et al. 2019, *Frontiers in Astronomy and Space Sciences*, 6, doi: [10.3389/fspas.2019.00023](https://doi.org/10.3389/fspas.2019.00023)

- Amano, T., Katou, T., Kitamura, N., et al. 2020, *Phys Rev Lett*, 124, 065101, doi: [10.1103/PhysRevLett.124.065101](https://doi.org/10.1103/PhysRevLett.124.065101)
- Ambrosiano, J., Matthaeus, W. H., Goldstein, M. L., & Plante, D. 1988, *Journal of Geophysical Research: Space Physics*, 93, 14383, doi: [10.1029/JA093iA12p14383](https://doi.org/10.1029/JA093iA12p14383)
- Angelopoulos, V., Baumjohann, W., Kennel, C. F., et al. 1992, *J Geophys Res-Space*, 97, 4027, doi: [Doi10.1029/91ja02701](https://doi.org/10.1029/91ja02701)
- Angelopoulos, V., Coroniti, F. V., Kennel, C. F., et al. 1996, *Journal of Geophysical Research: Space Physics*, 101, 4967, doi: [10.1029/95JA02722](https://doi.org/10.1029/95JA02722)
- Ansoldi, S., Antonelli, L. A., Antoranz, P., et al. 2016, *Astronomy & Astrophysics*, 585, doi: [10.1051/0004-6361/201526853](https://doi.org/10.1051/0004-6361/201526853)
- Araudo, A. T., Bell, A. R., Blundell, K. M., & Matthews, J. H. 2018, *Monthly Notices of the Royal Astronomical Society*, 473, 3500, doi: [10.1093/mnras/stx2552](https://doi.org/10.1093/mnras/stx2552)
- Araudo, A. T., Bell, A. R., Crilly, A., & Blundell, K. M. 2016, *Monthly Notices of the Royal Astronomical Society*, 460, 3554, doi: [10.1093/mnras/stw1204](https://doi.org/10.1093/mnras/stw1204)
- Artemyev, A. V., Zhang, X. J., Demekhov, A. G., et al. 2024, *Journal of Geophysical Research: Space Physics*, 129, doi: [10.1029/2023ja032287](https://doi.org/10.1029/2023ja032287)
- Asai, A., Masuda, S., Yokoyama, T., et al. 2002, *The Astrophysical Journal*, 578, L91, doi: [10.1086/344566](https://doi.org/10.1086/344566)
- Aschwanden, M. J. 2005, *Physics of the Solar Corona* (Springer Berlin Heidelberg), doi: [10.1007/3-540-30766-4](https://doi.org/10.1007/3-540-30766-4)
- . 2012, *Space Science Reviews*, 171, 3, doi: [10.1007/s11214-011-9865-x](https://doi.org/10.1007/s11214-011-9865-x)
- Aschwanden, M. J., Hudson, H., Kosugi, T., & Schwartz, R. A. 1996, *Astrophys J*, 464, 985, doi: [Doi10.1086/177386](https://doi.org/10.1086/177386)
- Atoyan, A. M., & Aharonian, F. A. 1996, *Monthly Notices of the Royal Astronomical Society*, 278, 525, doi: [10.1093/mnras/278.2.525](https://doi.org/10.1093/mnras/278.2.525)
- Bamba, A., Yamazaki, R., Ueno, M., & Koyama, K. 2003, *The Astrophysical Journal*, 589, 827, doi: [10.1086/374687](https://doi.org/10.1086/374687)
- Bamba, A., Fukazawa, Y., Hiraga, J. S., et al. 2008, *Publications of the Astronomical Society of Japan*, 60, S153, doi: [10.1093/pasj/60.sp1.S153](https://doi.org/10.1093/pasj/60.sp1.S153)
- Band, D., Matteson, J., Ford, L., et al. 1993, *The Astrophysical Journal*, 413, doi: [10.1086/172995](https://doi.org/10.1086/172995)
- Becker, H. N., Alexander, J. W., Connerney, J. E. P., et al. 2021, *Journal of Geophysical Research: Planets*, 126, doi: [10.1029/2020je006772](https://doi.org/10.1029/2020je006772)
- Bell, A. R. 2004, *Monthly Notices of the Royal Astronomical Society*, 353, 550, doi: [10.1111/j.1365-2966.2004.08097.x](https://doi.org/10.1111/j.1365-2966.2004.08097.x)
- Berezhko, E. G., Ksenofontov, L. T., & Völk, H. J. 2002, *Astronomy & Astrophysics*, 395, 943, doi: [10.1051/0004-6361:20021219](https://doi.org/10.1051/0004-6361:20021219)
- Bird, M. K., & Edenhofer, P. 1990, *Remote Sensing Observations of the Solar Corona* (Berlin Heidelberg: Springer-Verlag), 13–98
- Blake, J. B., Kolasinski, W. A., Fillius, R. W., & Mullen, E. G. 1992, *Geophysical Research Letters*, 19, 821, doi: [10.1029/92gl00624](https://doi.org/10.1029/92gl00624)
- Blandford, R., & Eichler, D. 1987, *Physics Reports*, 154, 1, doi: [10.1016/0370-1573\(87\)90134-7](https://doi.org/10.1016/0370-1573(87)90134-7)
- Bolton, S. J., Janssen, M., Thorne, R., et al. 2002, *Nature*, 415, 987, doi: [10.1038/415987a](https://doi.org/10.1038/415987a)
- Bowers, C. F., Jackman, C. M., Sun, W., et al. 2024, *Journal of Geophysical Research: Space Physics*, 129, doi: [10.1029/2023ja032162](https://doi.org/10.1029/2023ja032162)
- Buhler, R., & Blandford, R. 2014, *Rep Prog Phys*, 77, 066901, doi: [10.1088/0034-4885/77/6/066901](https://doi.org/10.1088/0034-4885/77/6/066901)
- Burlaga, L. F., Ness, N. F., Acuña, M. H., et al. 2008, *Nature*, 454, 75, doi: [10.1038/nature07029](https://doi.org/10.1038/nature07029)
- Carilli, C. L., & Barthel, P. D. 1996, *Astron Astrophys Rev*, 7, 1, doi: [10.1007/s001590050001](https://doi.org/10.1007/s001590050001)
- Carmichael, H. 1962, *Space Science Reviews*, 1, doi: [10.1007/bf00174635](https://doi.org/10.1007/bf00174635)
- Casse, F., & Marcowith, A. 2005, *Astroparticle Physics*, 23, 31, doi: [10.1016/j.astropartphys.2004.11.003](https://doi.org/10.1016/j.astropartphys.2004.11.003)
- Chen, Bastian, T. S., Shen, C., et al. 2015, *Science*, 350, 1238, doi: [10.1126/science.aac8467](https://doi.org/10.1126/science.aac8467)
- Chen, B., Shen, C. C., Gary, D. E., et al. 2020, *Nature Astronomy*, 4, 1140, doi: [10.1038/s41550-020-1147-7](https://doi.org/10.1038/s41550-020-1147-7)
- Chien, A., Gao, L., Zhang, S., et al. 2023, *Nat Phys*, doi: [10.1038/s41567-022-01839-x](https://doi.org/10.1038/s41567-022-01839-x)
- Christon, S. P., Mitchell, D. G., Williams, D. J., et al. 1988, *Journal of Geophysical Research*, 93, 2562, doi: [10.1029/JA093iA04p02562](https://doi.org/10.1029/JA093iA04p02562)
- Christon, S. P., Williams, D. J., Mitchell, D. G., Frank, L. A., & Huang, C. Y. 1989, *Journal of Geophysical Research*, 94, 13409, doi: [10.1029/JA094iA10p13409](https://doi.org/10.1029/JA094iA10p13409)
- Christon, S. P., Williams, D. J., Mitchell, D. G., Huang, C. Y., & Frank, L. A. 1991, *Journal of Geophysical Research*, 96, 1, doi: [10.1029/90ja01633](https://doi.org/10.1029/90ja01633)
- Cummings, A. C., & Stone, E. C. 1998, *Space Science Reviews*, 83, 51, doi: [10.1023/a:1005057010311](https://doi.org/10.1023/a:1005057010311)
- de Pater, I., & Dunn, D. E. 2003, *Icarus*, 163, 449, doi: [10.1016/s0019-1035\(03\)00068-x](https://doi.org/10.1016/s0019-1035(03)00068-x)
- Dewey, R. M., Raines, J. M., Sun, W., Slavin, J. A., & Poh, G. 2018, *Geophysical Research Letters*, 45, doi: [10.1029/2018gl079056](https://doi.org/10.1029/2018gl079056)
- Diesing, R. 2023, *The Astrophysical Journal*, 958, doi: [10.3847/1538-4357/ad00b1](https://doi.org/10.3847/1538-4357/ad00b1)
- Dmitruk, P., Matthaeus, W. H., Seenu, N., & Brown, M. R. 2003, *The Astrophysical Journal*, 597, L81, doi: [10.1086/379751](https://doi.org/10.1086/379751)
- Drake, J. F., Opher, M., Swisdak, M., & Chamoun, J. N. 2010, *The Astrophysical Journal*, 709, 963, doi: [10.1088/0004-637x/709/2/963](https://doi.org/10.1088/0004-637x/709/2/963)

- Drury, L. O. 2012, *Astroparticle Physics*, 39-40, 52, doi: [10.1016/j.astropartphys.2012.02.006](https://doi.org/10.1016/j.astropartphys.2012.02.006)
- Ellison, D. C., & Ramaty, R. 1985, *The Astrophysical Journal*, 298, doi: [10.1086/163623](https://doi.org/10.1086/163623)
- Evenson, P., Meyer, P., Yanagita, S., & Forrest, D. J. 1984, *The Astrophysical Journal*, 283, doi: [10.1086/162323](https://doi.org/10.1086/162323)
- Fairfield, D. H. 1971, *Journal of Geophysical Research*, 76, 6700, doi: [10.1029/JA076i028p06700](https://doi.org/10.1029/JA076i028p06700)
- Fairfield, D. H., & Jones, J. 1996, *Journal of Geophysical Research: Space Physics*, 101, 7785, doi: [10.1029/95ja03713](https://doi.org/10.1029/95ja03713)
- Feigelson, E. D., Laurent-Muehleisen, S. A., Kollgaard, R. I., & Fomalont, E. B. 1995, *The Astrophysical Journal*, 449, doi: [10.1086/309642](https://doi.org/10.1086/309642)
- Fischer, H. M., Pehlke, E., Wibberenz, G., Lanzerotti, L. J., & Mihalov, J. D. 1996, *Science*, 272, 856, doi: [10.1126/science.272.5263.856](https://doi.org/10.1126/science.272.5263.856)
- Fiuzza, F., Swadling, G. F., Grassi, A., et al. 2020, *Nat Phys*, 16, 916, doi: [10.1038/s41567-020-0919-4](https://doi.org/10.1038/s41567-020-0919-4)
- Fukui, Y., Sano, H., Yamane, Y., et al. 2021, *The Astrophysical Journal*, 915, doi: [10.3847/1538-4357/abff4a](https://doi.org/10.3847/1538-4357/abff4a)
- Gardner, F. F., & Milne, D. K. 1965, *The Astronomical Journal*, 70, doi: [10.1086/109813](https://doi.org/10.1086/109813)
- Gershman, D. J., Fuselier, S. A., Cohen, I. J., et al. 2024, *Space Science Reviews*, 220, doi: [10.1007/s11214-023-01017-2](https://doi.org/10.1007/s11214-023-01017-2)
- Giacalone, J., Fahr, H., Fichtner, H., et al. 2022, *Space Science Reviews*, 218, doi: [10.1007/s11214-022-00890-7](https://doi.org/10.1007/s11214-022-00890-7)
- Goldreich, P., & Julian, W. H. 1969, *The Astrophysical Journal*, 157, doi: [10.1086/150119](https://doi.org/10.1086/150119)
- Goldstein, M. L., Matthaues, W. H., & Ambrosiano, J. J. 1986, *Geophysical Research Letters*, 13, 205, doi: [10.1029/GL013i003p00205](https://doi.org/10.1029/GL013i003p00205)
- Green, D. A. 2019, *Journal of Astrophysics and Astronomy*, 40, doi: [10.1007/s12036-019-9601-6](https://doi.org/10.1007/s12036-019-9601-6)
- Guo, F., Liu, Y.-H., Zenitani, S., & Hoshino, M. 2024, *Space Science Reviews*, 220, doi: [10.1007/s11214-024-01073-2](https://doi.org/10.1007/s11214-024-01073-2)
- Guo, J., Li, X., Zhang, J., et al. 2023, *Geophysical Research Letters*, 50, doi: [10.1029/2023gl103069](https://doi.org/10.1029/2023gl103069)
- Guo, R., & Yao, Z. 2024, *Reviews of Modern Plasma Physics*, 8, doi: [10.1007/s41614-024-00162-7](https://doi.org/10.1007/s41614-024-00162-7)
- Hairston, M. R., Drake, K. A., & Skoug, R. 2005, *Journal of Geophysical Research: Space Physics*, 110, doi: [10.1029/2004ja010864](https://doi.org/10.1029/2004ja010864)
- Hess, W. N. 1959, *Physical Review Letters*, 3, 11, doi: [10.1103/PhysRevLett.3.11](https://doi.org/10.1103/PhysRevLett.3.11)
- Hill, T. W., Thomsen, M. F., Henderson, M. G., et al. 2008, *Journal of Geophysical Research: Space Physics*, 113, doi: [10.1029/2007ja012626](https://doi.org/10.1029/2007ja012626)
- Hillas, a. M. 1984, *Annual Review of Astronomy and Astrophysics*, 22, 425, doi: [10.1146/annurev.aa.22.090184.002233](https://doi.org/10.1146/annurev.aa.22.090184.002233)
- Hillas, A. M. 2005, *Journal of Physics G: Nuclear and Particle Physics*, 31, R95, doi: [10.1088/0954-3899/31/5/r02](https://doi.org/10.1088/0954-3899/31/5/r02)
- Ho, G. C., Krimigis, S. M., Gold, R. E., et al. 2011, *Science*, 333, 1865, doi: [10.1126/science.1211141](https://doi.org/10.1126/science.1211141)
- . 2012, *Journal of Geophysical Research: Space Physics*, 117, doi: [10.1029/2012ja017983](https://doi.org/10.1029/2012ja017983)
- Jackman, C. M., Thomsen, M. F., & Dougherty, M. K. 2019, *Journal of Geophysical Research: Space Physics*, 124, 8865, doi: [10.1029/2019ja026628](https://doi.org/10.1029/2019ja026628)
- Jackman, C. M., Arridge, C. S., André, N., et al. 2014, *Space Science Reviews*, 182, 85, doi: [10.1007/s11214-014-0060-8](https://doi.org/10.1007/s11214-014-0060-8)
- Jaynes, A. N., Baker, D. N., Singer, H. J., et al. 2015, *Journal of Geophysical Research: Space Physics*, 120, 7240, doi: [10.1002/2015ja021234](https://doi.org/10.1002/2015ja021234)
- Jokipii, J. R. 1987, *Astrophys J*, 313, 842, doi: [Doi10.1086/165022](https://doi.org/10.1086/165022)
- Jokipii, J. R., & Giacalone, J. 1998, *Space Science Reviews*, 83, 123, doi: [10.1023/a:1005077629875](https://doi.org/10.1023/a:1005077629875)
- Kahler, S. 1994, *The Astrophysical Journal*, 428, doi: [10.1086/174292](https://doi.org/10.1086/174292)
- Kaneda, H., Tashiro, M., Ikebe, Y., et al. 1995, *The Astrophysical Journal*, 453, doi: [10.1086/309742](https://doi.org/10.1086/309742)
- Katsuda, S., Petre, R., Long, K. S., et al. 2009, *The Astrophysical Journal*, 692, L105, doi: [10.1088/0004-637x/692/2/l105](https://doi.org/10.1088/0004-637x/692/2/l105)
- Kennel, C. F., & Coroniti, F. V. 1984, *The Astrophysical Journal*, 283, doi: [10.1086/162356](https://doi.org/10.1086/162356)
- Kivelson, M. G., & Khurana, K. K. 2002, *Journal of Geophysical Research: Space Physics*, 107, doi: [10.1029/2001ja000249](https://doi.org/10.1029/2001ja000249)
- Kliem, B. 1994, *Astrophys J Suppl S*, 90, 719, doi: [10.1086/191896](https://doi.org/10.1086/191896)
- Kollmann, P., Paranicas, C., Clark, G., et al. 2017, *Geophysical Research Letters*, 44, 5259, doi: [10.1002/2017gl073730](https://doi.org/10.1002/2017gl073730)
- Kotera, K., & Olinto, A. V. 2011, *Annual Review of Astronomy and Astrophysics*, 49, 119, doi: [10.1146/annurev-astro-081710-102620](https://doi.org/10.1146/annurev-astro-081710-102620)
- Koyama, K., Petre, R., Gotthelf, E. V., et al. 1995, *Nature*, 378, 255, doi: [DOI10.1038/378255a0](https://doi.org/10.1038/378255a0)
- Krimigis, S. M. 1979, *AIP Conference Proceedings*, 56, 179, doi: [10.1063/1.32079](https://doi.org/10.1063/1.32079)
- Kronberg, E. A., Woch, J., Krupp, N., & Lagg, A. 2008, *Journal of Geophysical Research: Space Physics*, 113, doi: [10.1029/2008ja013332](https://doi.org/10.1029/2008ja013332)
- Krucker, S., Battaglia, M., Cargill, P. J., et al. 2008, *Astron Astrophys Rev*, 16, 155, doi: [10.1007/s00159-008-0014-9](https://doi.org/10.1007/s00159-008-0014-9)
- Krupp, N., Roussos, E., Kollmann, P., et al. 2018, *Geophysical Research Letters*, 45, doi: [10.1029/2018gl078096](https://doi.org/10.1029/2018gl078096)
- Lagage, P. O., & Cesarsky, C. J. 1983, *Astronomy & Astrophysics*, 125, 249
- Larrodera, C., & Cid, C. 2020, *Astronomy & Astrophysics*, 635, doi: [10.1051/0004-6361/201937307](https://doi.org/10.1051/0004-6361/201937307)

- Singer, S. F. 1958a, *Physical Review Letters*, 1, 171, doi: [10.1103/PhysRevLett.1.171](https://doi.org/10.1103/PhysRevLett.1.171)
- . 1958b, *Physical Review Letters*, 1, 181, doi: [10.1103/PhysRevLett.1.181](https://doi.org/10.1103/PhysRevLett.1.181)
- Slavin, J. A., Imber, S. M., Boardsen, S. A., et al. 2012, *Journal of Geophysical Research: Space Physics*, 117, doi: [10.1029/2012ja017926](https://doi.org/10.1029/2012ja017926)
- Smart, D. F., & Shea, M. A. 1985, *J Geophys Res-Space*, 90, 183, doi: [DOI10.1029/JA090iA01p00183](https://doi.org/DOI10.1029/JA090iA01p00183)
- Smith, A. W., Jackman, C. M., & Thomsen, M. F. 2016, *J Geophys Res Space Phys*, 121, 2984, doi: [10.1002/2015JA022005](https://doi.org/10.1002/2015JA022005)
- Sorathia, K. A., Ukhorskiy, A. Y., Merkin, V. G., Fennell, J. F., & Claudepierre, S. G. 2018, *Journal of Geophysical Research: Space Physics*, 123, 5590, doi: [10.1029/2018ja025506](https://doi.org/10.1029/2018ja025506)
- Steenbrugge, K. C., & Blundell, K. M. 2008, *Monthly Notices of the Royal Astronomical Society*, 388, 1457, doi: [10.1111/j.1365-2966.2007.12665.x](https://doi.org/10.1111/j.1365-2966.2007.12665.x)
- Suzuki, H., Bamba, A., Yamazaki, R., & Ohira, Y. 2022, *The Astrophysical Journal*, 924, doi: [10.3847/1538-4357/ac33b5](https://doi.org/10.3847/1538-4357/ac33b5)
- Takahashi, T., Tanaka, T., Uchiyama, Y., et al. 2008, *Publications of the Astronomical Society of Japan*, 60, S131, doi: [10.1093/pasj/60.sp1.S131](https://doi.org/10.1093/pasj/60.sp1.S131)
- Tanaka, T., Uchida, H., Sano, H., & Tsuru, T. G. 2020, *The Astrophysical Journal Letters*, 900, doi: [10.3847/2041-8213/abaef0](https://doi.org/10.3847/2041-8213/abaef0)
- Tao, M., Kataoka, J., & Tanaka, T. 2024, *The Astrophysical Journal Letters*, 970, doi: [10.3847/2041-8213/ad60c7](https://doi.org/10.3847/2041-8213/ad60c7)
- Terasawa, T. 2001, *Science and Technology of Advanced Materials*, 2, 461, doi: [10.1016/s1468-6996\(01\)00144-9](https://doi.org/10.1016/s1468-6996(01)00144-9)
- . 2011, *Proceedings of the International Astronomical Union*, 6, 214, doi: [10.1017/s174392131100696x](https://doi.org/10.1017/s174392131100696x)
- Terasawa, T., & Nishida, A. 1976, *Planetary and Space Science*, 24, 855, doi: [10.1016/0032-0633\(76\)90076-3](https://doi.org/10.1016/0032-0633(76)90076-3)
- Thomsen, M. F., Jackman, C. M., & Lamy, L. 2019, *Journal of Geophysical Research: Space Physics*, 124, 7799, doi: [10.1029/2019ja026819](https://doi.org/10.1029/2019ja026819)
- Trattner, K. J., Fuselier, S. A., Schwartz, S. J., et al. 2023, *Journal of Geophysical Research: Space Physics*, 128, doi: [10.1029/2022ja030631](https://doi.org/10.1029/2022ja030631)
- Tsuji, N., & Uchiyama, Y. 2016, *Publications of the Astronomical Society of Japan*, doi: [10.1093/pasj/psw102](https://doi.org/10.1093/pasj/psw102)
- Tsuji, N., Uchiyama, Y., Aharonian, F., et al. 2019, *The Astrophysical Journal*, 877, doi: [10.3847/1538-4357/ab1b29](https://doi.org/10.3847/1538-4357/ab1b29)
- Tsuneta, S., & Naito, T. 1998, *The Astrophysical Journal*, 495, L67, doi: [10.1086/311207](https://doi.org/10.1086/311207)
- Turner, D. L., Wilson, L. B., r., Liu, T. Z., et al. 2018, *Nature*, 561, 206, doi: [10.1038/s41586-018-0472-9](https://doi.org/10.1038/s41586-018-0472-9)
- Turner, D. L., Cohen, I. J., Michael, A., et al. 2021, *Geophysical Research Letters*, 48, doi: [10.1029/2021gl095495](https://doi.org/10.1029/2021gl095495)
- Uchiyama, Y., Aharonian, F. A., Tanaka, T., Takahashi, T., & Maeda, Y. 2007, *Nature*, 449, 576, doi: [10.1038/nature06210](https://doi.org/10.1038/nature06210)
- Vampola, A. L., & Korth, A. 1992, *Geophysical Research Letters*, 19, 625, doi: [10.1029/92gl00121](https://doi.org/10.1029/92gl00121)
- Vashenyuk, E. V., Balabin, Y. V., & Gvozdevsky, B. B. 2011, *Astrophysics and Space Sciences Transactions*, 7, 459, doi: [10.5194/astra-7-459-2011](https://doi.org/10.5194/astra-7-459-2011)
- Vasyliunas, V. M. 1983, *Plasma distribution and flow* (Cambridge University Press), 395–453, doi: [10.1017/CBO9780511564574.013](https://doi.org/10.1017/CBO9780511564574.013)
- Vilmer, N., MacKinnon, A. L., Trotter, G., & Barat, C. 2003, *Astronomy & Astrophysics*, 412, 865, doi: [10.1051/0004-6361:20031488](https://doi.org/10.1051/0004-6361:20031488)
- Vogt, M. F., Kivelson, M. G., Khurana, K. K., Joy, S. P., & Walker, R. J. 2010, *Journal of Geophysical Research: Space Physics*, 115, doi: [10.1029/2009ja015098](https://doi.org/10.1029/2009ja015098)
- Vogt, M. F., Connerney, J. E. P., DiBraccio, G. A., et al. 2020, *J Geophys Res Space Phys*, 125, doi: [10.1029/2019ja027486](https://doi.org/10.1029/2019ja027486)
- Weisskopf, M. C., Hester, J. J., Tennant, A. F., et al. 2000, *Astrophys J*, 536, L81, doi: [10.1086/312733](https://doi.org/10.1086/312733)
- Wilson, L. B., Sibeck, D. G., Turner, D. L., et al. 2016, *Physical Review Letters*, 117, 215101, doi: [ARTN21510110.1103/PhysRevLett.117.215101](https://doi.org/ARTN21510110.1103/PhysRevLett.117.215101)
- Winkler, P. F., Gupta, G., & Long, K. S. 2003, *The Astrophysical Journal*, 585, 324, doi: [10.1086/345985](https://doi.org/10.1086/345985)
- Winslow, R. M., Anderson, B. J., Johnson, C. L., et al. 2013, *J Geophys Res-Space*, 118, 2213, doi: [10.1002/jgra.50237](https://doi.org/10.1002/jgra.50237)
- Yaji, Y., Tashiro, M. S., Isobe, N., et al. 2010, *The Astrophysical Journal*, 714, 37, doi: [10.1088/0004-637x/714/1/37](https://doi.org/10.1088/0004-637x/714/1/37)
- Yamazaki, R., Yoshida, T., Terasawa, T., Bamba, A., & Koyama, K. 2004, *Astronomy & Astrophysics*, 416, 595, doi: [10.1051/0004-6361:20034212](https://doi.org/10.1051/0004-6361:20034212)
- Yao, W., Fazzini, A., Chen, S. N., et al. 2021, *Nat Phys*, 17, 1177, doi: [10.1038/s41567-021-01325-w](https://doi.org/10.1038/s41567-021-01325-w)
- Yeung, P. K. H. 2020, *Astronomy & Astrophysics*, 640, doi: [10.1051/0004-6361/202038166](https://doi.org/10.1051/0004-6361/202038166)
- Yuan, Q., Liu, S., Fan, Z., Bi, X., & Fryer, C. L. 2011, *The Astrophysical Journal*, 735, doi: [10.1088/0004-637x/735/2/120](https://doi.org/10.1088/0004-637x/735/2/120)
- Zank, G. P., le Roux, J. A., Webb, G. M., Dosch, A., & Khabarova, O. 2014, *The Astrophysical Journal*, 797, 28, doi: [10.1088/0004-637x/797/1/28](https://doi.org/10.1088/0004-637x/797/1/28)
- Zank, G. P., Hunana, P., Mostafavi, P., et al. 2015, *The Astrophysical Journal*, 814, 137, doi: [10.1088/0004-637x/814/2/137](https://doi.org/10.1088/0004-637x/814/2/137)
- Zhang, L. Q., Baumjohann, W., Wang, C., Dai, L., & Tang, B. B. 2016, *Journal of Geophysical Research: Space Physics*, 121, 8773, doi: [10.1002/2016ja022397](https://doi.org/10.1002/2016ja022397)
- Zhang, X., Chen, Y., Huang, J., & Chen, D. 2020, *Monthly Notices of the Royal Astronomical Society*, 497, 3477, doi: [10.1093/mnras/staa2151](https://doi.org/10.1093/mnras/staa2151)